Orbital and spin order in oxide two-dimensional electron gases

John R. Tolsma,[1,*] Marco Polini,[2] and Allan H. MacDonald[1]
[1]*Department of Physics, The University of Texas at Austin, Austin, Texas 78712, USA*
[2]*Istituto Italiano di Tecnologia, Graphene Labs, Via Morego 30, I-16163 Genova, Italy*
(Received 12 August 2016; revised manuscript received 20 March 2017; published 2 May 2017)

We describe a variational theory of multiband two-dimensional electron gases that captures the interplay between electrostatic confining potentials, orbital-dependent interlayer electronic hopping, and electron-electron interactions and apply it to the d-band two-dimensional electron gases that form near perovskite oxide surfaces and heterojunctions. These multiband two-dimensional electron gases are prone to the formation of Coulomb-interaction-driven orbitally-ordered nematic ground states. We find that as the electron density is lowered and interaction effects strengthen, spontaneous orbital order occurs first, followed by spin order. We compare our results with known properties of single-component two-dimensional electron gas systems and comment on closely related physics in semiconductor quantum wells and van der Waals heterostructures.

DOI: 10.1103/PhysRevB.95.205101

I. INTRODUCTION

Orbital and spin order are relatively ubiquitous in strongly interacting systems, and have long been studied in ABO_3 bulk crystals with the perovskite crystal structure [1,2]. In perovskites B is typically a transition metal and A is either an alkaline or rare earth metal. Among these materials, those with partially filled transition metal t_{2g} d orbitals are particularly interesting because orbital and spin order appear almost simultaneously near the magnetic transition temperature [3–5]. As a consequence of relatively recent advances [6–10] it is now possible to add electrons to quantum wells formed by d^0 perovskites, most commonly $SrTiO_3$. The resulting systems are two-dimensional metals with far fewer than one conduction electron per transition metal site. In this paper we address orbital and spin order and their interplay in these new low carrier-density perovskite quantum well systems.

This paper describes a theoretical approach that is intended to be useful for t_{2g} two-dimensional gases formed at interfaces or in quantum wells. It is motivated by the desirability of capturing the essentially two-dimensional character of electronic correlations in these systems, while accounting at the same time for the influence of those correlations on confinement properties and subband energy alignment. Because the number of d electrons per unit cell is small in the systems of interest, it is essential to account for the long range of the Coulomb interactions between electrons. This feature of the problem is shared between t_{2g} electron gases and the familiar electron gases formed in covalent semiconductor quantum wells and contrasts with the case of d-electron two-dimensional electron gases with densities comparable to or larger than one conduction electron per unit cell. In the latter case, the number of t_{2g} electrons per transition metal is close to one, the probability of two electrons occupying the same site is substantial, and short-range Hubbard-type interaction models normally capture the most important parts of the interaction physics [11,12]; generalizations of the Hubbard model apply for larger integer values of the number of electrons per metal atom.

Because of its long range, the typical Coulomb interaction energy of an individual electron in these systems drops to zero only as two-dimensional density $n^{1/2}$, in contrast to the $\sim n$ behavior which would be obtained by applying an artificial Hubbard model [13]. Indeed, the probability that a pair of electrons will occupy the same unit cell is reduced below statistical values by electronic correlations that have little kinetic energy competition at such low densities. It follows that the interaction physics in these systems is controlled by the full long-range Coulomb interaction, which must be retained in order to achieve a realistic description of electron-electron interaction effects [14]. The same reasoning applies to theories of correlations among low-energy electrons in other systems with far less than one electron per unit cell, e.g., semimetals and doped semiconductors.

Unlike most semiconductor based two-dimensional electron gases, however, transition-metal oxide based 2DEGs have conduction bands formed from spatially localized atomic d orbitals which have small interatom hopping amplitudes and subsequently large electron effective masses. As a result, nearly all experimentally accessible densities are in a regime where the Coulomb interaction energy per electron is large compared to the kinetic energy per electron. In addition, while some semiconductor based 2DEGs occupy several valleys in momentum space, which is in some ways a reasonable analog of the multiple low-energy bands present in oxide based 2DEGs (see below), the latter are formed from d orbitals with highly anisotropic hopping amplitudes which leads to features which are qualitatively new to the field of electron gas physics, e.g., anisotropic Fermi surfaces, significant band-edge energy differences, and large variations in the spatial confinement of different bands to interfaces and heterojunctions. At this time it is not known whether these features will give rise to qualitatively new phenomena, but opportunities for exploring the impact of strong Coulomb interactions in this landscape are clearly abundant.

As already mentioned, in this paper we focus on understanding the possibility of orbital and spin order and their interplay in $SrTiO_3$ based 2DEGs. The possibility of spin order in electron gases with a single parabolic band was raised very early in the history of the quantum theory of solids [15]. Although many experiments have hinted at ferromagnetic

*tolsma@physics.utexas.edu

instabilities in these single-band electron gas systems [16–21], unambiguous evidence for magnetism has so far been lacking. Theoretically, order is expected only at extremely low carrier densities, at least in the absence of disorder [22–24]. In our study we capture the peculiarities of perovskite multiband two-dimensional electron gas systems in the hopes of opening up a richer range of experimental possibilities for observing these broken symmetry states. We predict that strong Coulomb interactions, large band-edge offsets, and band-dependent interfacial confinement combine to endow the $SrTiO_3$ 2DEG with a strong instability toward the formation of orbital and spin ordered states at experimentally accessible densities.

In the following sections we will detail how the study of spin and orbital instabilities requires a new theoretical approach. In multiband two-dimensional electron gas heterojunctions and quantum wells, the ground-state energy depends sensitively on the density in each spin-resolved band. We propose a modified variational theory which captures the interplay between orbital-dependent interlayer electronic hopping, the electrostatic confining potential, and electron-electron interactions. Our theory attempts to capture physics that is missing in most density-functional theory [25,26] calculations which typically employ an extended version of the local-density approximation (LDA) for the exchange-correlation (XC) energy functional,

$$E_{\rm XC}^{\rm LDA}[n(\boldsymbol{r})] = \int d\boldsymbol{r}\, n(\boldsymbol{r})\, \xi_{\rm XC}(n(\boldsymbol{r})), \tag{1}$$

where $\xi_{\rm XC}(n(\boldsymbol{r}))$ is the XC energy-per-electron of the single-band isotropic electron gas model with homogeneously distributed electron density $n(\boldsymbol{r})$. Despite its great success, it is generally known that the LDA and its generalizations (e.g., the generalized gradient approximation [27,28]) do not in all cases adequately describe the XC energy. In covalent semiconductors, this shortcoming is highlighted by a significant underestimation of the band-gap energy. This limitation can be traced back to Eq. (1), where we see that the LDA XC energy functional is sensitive to the local electron density but not to the orbital symmetries of the occupied electronic states [29,30]. Hybrid density-functional theory (see for example Refs. [31] and [32]) tries to overcome this by using linear combinations of the Hartree-Fock exchange energy with a traditional XC energy functional, but is both computationally expensive and often works best when the relative weights in the linear combination of energy functionals are determined by experiment. Here we take a different approach. Motivated by an interest in orbital and spin order in t_{2g} two-dimensional electron gases, we have developed a broadly applicable variational theory for the ground-state energy which is sensitive to the electron density in each band and therefore is sensitive to electron orbital symmetry in systems in which each band has a dominant orbital character. Although we here use the variational theory to study perovskite oxide 2DEGs, we further discuss in the final section of this paper that the method is generally applicable to calculate the ground-state energy and related quantities (e.g., thermodynamic observables, spin and valley susceptibilities, etc.) in semiconducting parabolic-band quantum wells and multilayered van der Waals heterostructures.

Our paper is organized as follows. In Sec. II we briefly summarize the t_{2g} 2DEG model we have introduced previously [14] and extend it to account explicitly for the concerted action of orbital-dependent electronic hopping along the confinement direction and electron-electron interactions. In Sec. III we describe a variational approximation for the ground state that accounts self-consistently for interfacial confinement forces and their influence on XC energies. As a first application of this method, we calculate the phase diagram for the t_{2g} 2DEG as a function of total density and quantum well thickness in Sec. IV. We show that Coulomb interactions give rise to a novel sequence of orbital- and spin-ordered ground states, with correlations favoring the former. Compared to the single-component isotropic 2DEG case, the t_{2g} 2DEG is dramatically more susceptible to these Bloch-like [15] instabilities. We comment on the experimental signatures of these states and suggest possible extensions of the calculations presented here. Finally, in Section V we summarize our results and comment on the applicability of our variational approximation to semiconductor quantum wells, van der Waals heterostructures, and other multicomponent 2D electron systems.

II. t_{2g} ELECTRON GAS MODEL

We begin by summarizing the simple model for the low-energy conduction bands in $SrTiO_3$ quantum wells and heterojunctions that we study. We first separate the noninteracting part of the Hamiltonian into two sets of terms: those which describe electronic motion parallel ($\parallel$) to the confinement direction, and those which describe electronic motion perpendicular ($\perp$) to the confinement direction, which we take to be the $\hat{\boldsymbol{z}}$ direction. The purpose of this separation will become clear in Sec. III.

The band structure of $SrTiO_3$ electron gases has been thoroughly discussed in the literature [33–35]. Here we briefly describe some details required for the present analysis. The low-energy conduction bands of $SrTiO_3$ quantum wells and heterojunctions are formed from the xy, yz, and xz d orbitals (the t_{2g} orbitals) of Ti. $SrTiO_3$ has a perovskite crystal structure, but the sublattice formed by the Ti atoms is simple cubic and described by the lattice vector $\boldsymbol{R} = a(n_x\hat{\boldsymbol{x}} + n_y\hat{\boldsymbol{y}} + n_z\hat{\boldsymbol{z}})$ where $a = 3.9$ Å is the lattice constant of $SrTiO_3$. Orbital symmetry dictates that each t_{2g} electron hops mainly between states with the same orbital character, with a large hopping amplitude t in the two directions in the plane of the orbital, and a smaller hopping amplitude t' in the third direction [34]. The weak hopping directions for xy, xz, and yz orbitals are $\hat{\boldsymbol{z}}$, $\hat{\boldsymbol{y}}$, and $\hat{\boldsymbol{x}}$, respectively. Nearest neighbor hopping on the simple-cubic Ti sublattice is described by the noninteracting Hamiltonian

$$\mathcal{H}_0 = \sum_{\alpha\sigma}\sum_{\boldsymbol{R}\boldsymbol{R}'} c^{\dagger}_{\boldsymbol{R}\alpha\sigma}\, h_{\alpha}(\boldsymbol{R}-\boldsymbol{R}')\, c_{\boldsymbol{R}'\alpha\sigma}, \tag{2}$$

where

$$h_{\alpha}(\boldsymbol{R}-\boldsymbol{R}') = \begin{cases} -t\delta_{\Delta\boldsymbol{R},\pm a\hat{\boldsymbol{x}}} - t\delta_{\Delta\boldsymbol{R},\pm a\hat{\boldsymbol{y}}} - t'\delta_{\Delta\boldsymbol{R},\pm a\hat{\boldsymbol{z}}} & \text{for} \quad \alpha = xy \\ -t\delta_{\Delta\boldsymbol{R},\pm a\hat{\boldsymbol{x}}} - t'\delta_{\Delta\boldsymbol{R},\pm a\hat{\boldsymbol{y}}} - t\delta_{\Delta\boldsymbol{R},\pm a\hat{\boldsymbol{z}}} & \text{for} \quad \alpha = xz \\ -t'\delta_{\Delta\boldsymbol{R},\pm a\hat{\boldsymbol{x}}} - t\delta_{\Delta\boldsymbol{R},\pm a\hat{\boldsymbol{y}}} - t\delta_{\Delta\boldsymbol{R},\pm a\hat{\boldsymbol{z}}} & \text{for} \quad \alpha = yz, \end{cases} \tag{3}$$

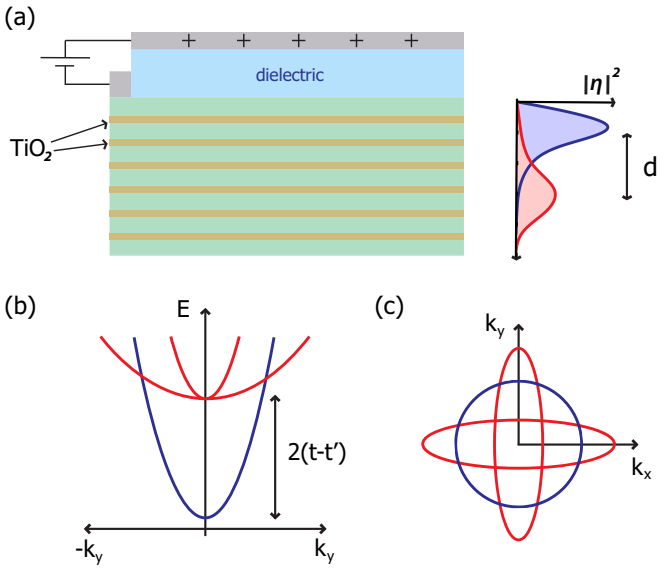

FIG. 1. A schematic summary of the t_{2g} 2DEG model for $SrTiO_3$. (a) At left is a top-gated $SrTiO_3$ heterojunction which hosts t_{2g} electrons distributed across two-dimensional TiO_2 layers highlighted in orange. At right is a sketch of the squared amplitude of the subband wave functions, $|\eta|^2$, for the t_{2g} 2DEG model described in Sec. II. The xz and yz subband wave functions are shown in red and the xy subband wave function in blue, illustrating the difference between their interfacial confinements. The energy offset, equal to $2(t-t')$ in the single-layer limit, between the anisotropic xz and yz (red) band edges and the isotropic xy (blue) band edge is illustrated in (b) and the anisotropy of the elliptical xz and yz Fermi surfaces (red) is contrasted with the xy band's circular Fermi surface (blue) in (c). t and t' are, respectively, the large and small hopping amplitudes for t_{2g} orbitals discussed in the main text.

where the electron spin is labeled by σ and we have defined $\Delta\boldsymbol{R} = \boldsymbol{R} - \boldsymbol{R}'$.

2DEGs have been realized in δ-doped $SrTiO_3$ [8], in ionic-liquid gated $SrTiO_3$ [36], at heterojunctions between $SrTiO_3$ and polar perovskites [37–39], and in electrostatically gated $SrTiO_3$ [40]. For definiteness, we consider a $SrTiO_3$ heterojunction extending from $z = 0$ to $z = a(N_l + 1)$ with an electrical gate placed at $z < 0$. Here, N_l is the number of TiO_2 layers (see Fig. 1) with appreciable occupation. Electron motion in the plane perpendicular to the $\hat{z}$ direction is unbounded and Bloch bands are formed from t_{2g}-orbital hopping on the square Ti 2D sublattices. Electron creation operators in real and 2D momentum space are related by

$$c^\dagger_{\boldsymbol{R}\alpha\sigma} = \frac{1}{\sqrt{N}}\sum_{\boldsymbol{k}} e^{-i\boldsymbol{k}\cdot\boldsymbol{R}_\perp} c^\dagger_{\boldsymbol{k}R_z\alpha\sigma}, \tag{4}$$

where $\boldsymbol{R}_\perp$ ranges over the 2D square lattice projection of the Ti simple-cubic lattice, and $\boldsymbol{k}$ is a crystal momentum in the corresponding 2D Brillouin-zone.

With this notation, the noninteracting Hamiltonian can then be written as $\mathcal{H}_0 = \mathcal{T}^\parallel + \mathcal{T}^\perp$, where the interlayer hopping term is

$$\mathcal{T}^\parallel = \sum_{\alpha\sigma}\sum_{\boldsymbol{k}R_zR'_z} c^\dagger_{\boldsymbol{k}R_z\alpha\sigma}\, h^\parallel_\alpha(R_z - R'_z)\, c_{\boldsymbol{k}R'_z\alpha\sigma}, \tag{5}$$

with

$$h^\parallel_\alpha(R_z - R'_z) = \begin{cases} -t'\,\delta_{R_z-R'_z,\pm a\hat{z}} & \text{for} \quad \alpha = xy \\ -t\,\delta_{R_z-R'_z,\pm a\hat{z}} & \text{for} \quad \alpha = xz \\ -t\,\delta_{R_z-R'_z,\pm a\hat{z}} & \text{for} \quad \alpha = yz, \end{cases} \tag{6}$$

and the intralayer hopping term is

$$\mathcal{T}^\perp = \sum_{\alpha\sigma}\sum_{\boldsymbol{k}R_z} c^\dagger_{\boldsymbol{k}R_z\alpha\sigma}\, h^\perp_\alpha(\boldsymbol{k})\, c_{\boldsymbol{k}R_z\alpha\sigma} \tag{7}$$

with

$$h^\perp_\alpha(\boldsymbol{k}) = \begin{cases} \frac{\hbar^2k^2}{2m_{\rm L}} - 4t & \text{for} \quad \alpha = xy \\ \frac{\hbar^2k_x^2}{2m_{\rm L}} + \frac{\hbar^2k_y^2}{2m_{\rm H}} - 2(t+t') & \text{for} \quad \alpha = xz \\ \frac{\hbar^2k_x^2}{2m_{\rm H}} + \frac{\hbar^2k_y^2}{2m_{\rm L}} - 2(t+t') & \text{for} \quad \alpha = yz \end{cases}. \tag{8}$$

In using Eq. (8) we are assuming that the number of electrons per Ti atom is much less than one, a condition that is violated only in very narrow quantum well systems [41,42], so that only states near the Γ point of the 2D Brillouin zone are occupied. The energy dispersion of the conduction bands can be described using effective masses, which we obtain by expanding about Γ to leading order in $\boldsymbol{k}$. Equation (8) shows that the xz and yz bands have one heavy mass, $m_{\rm H}$, and one light mass, $m_{\rm L}$, while the xy band is isotropic and has a light mass $m_{\rm L}$ in both the x and y directions. In terms of the original hopping amplitudes, $m_{\rm H} = \hbar^2/(2t'a^2)$ and $m_{\rm L} = \hbar^2/(2ta^2)$.

In heterojunction systems, several xy, yz, and xz type subbands are expected to be occupied even at moderate electron densities [33–35]. However, since $\gtrsim 75\%$ of the electron density is contained in the lowest xy, yz, and xz subbands [34], we address the case in which only one subband of each orbital type is retained. This truncation is sufficiently realistic to account for the most interesting properties of heterojunction 2DEGs. The assumption can easily be relaxed when there is an interest in quantitatively describing the properties of particular 2DEG systems that have more occupied subbands. With this assumption Eq. (7) can be written as

$$\mathcal{T}^\perp = \sum_{\boldsymbol{k}\alpha\sigma} c^\dagger_{\boldsymbol{k}\alpha\sigma}\, h^\perp_\alpha(\boldsymbol{k})\, c_{\boldsymbol{k}\alpha\sigma}, \tag{9}$$

where α is an orbital label. Equation (8) gives the bare band dispersions for the three bands retained in our model, which are plotted in Fig. 1. According to recent tight-binding fits [34] to Shubnikov-de Haas measurements [43] of bulk n-type $SrTiO_3$, $t = 236$ meV, and $t' = 35$ meV so that

$$\frac{m_{\rm H}}{m} = \frac{\rm Ry}{t'}\left(\frac{a_{\rm B}}{a}\right)^2 \sim 7 \tag{10}$$

and

$$\frac{m_{\rm L}}{m} = \frac{\rm Ry}{t}\left(\frac{a_{\rm B}}{a}\right)^2 \sim 1, \tag{11}$$

where m is the bare electron mass, $a_{\rm B}$ is the Bohr radius, and Ry is the Rydberg energy unit.

The isolated-layer bare-electron Hamiltonian in Eq. (7) has several important qualitative features that are schematically depicted in Fig. 1. First, the xz and yz bands have elliptical Fermi surfaces, while the xy band is isotropic. Second, the xz and yz band edge is higher in energy than the xy band edge by $2(t-t') \sim 402$ meV when carriers are confined to a single

atomic layer. This offset will decrease as the electrons spread out in the confinement direction, but the quantum confinement energy will always be lower for xy orbitals. Because the xy band electrons have a much weaker hopping amplitude in the $\hat{z}$ direction (t') than the xz and yz electrons (t), they are more strongly confined to interfaces in heterojunction systems. We note that it is possible [14,44] to crudely account for the difference in interfacial confinement by introducing a parameter d, which is defined as the difference between xz, yz subbands, and the xy subband average $\hat{z}$-direction positions (see Fig. 1), however in the current paper we do not make this simplifying approximation.

Next we add electron-electron interactions to our Hamiltonian. When the electron density per Ti atom is much smaller than one, the Fermi surface occupies a small fraction of the Brillouin zone and the probability of two electrons simultaneously occupying the same Ti site is very small. In this limit, including only the Hubbard part of the full electron-electron interaction misses the most important Coulomb interactions [14]. Because of its long range, the typical Coulomb interaction energy of an individual electron vanishes only as two-dimensional density $n^{1/2}$, in contrast to the $\sim n$ scaling of the Hubbard model. We therefore include in our model calculations the full Coulomb interaction

$$\mathcal{V} = \frac{1}{2}\sum_{i\neq j}\frac{e^2/\kappa}{\sqrt{(\boldsymbol{r}_{\perp,i}-\boldsymbol{r}_{\perp,j})^2+(z_i-z_j)^2}}. \tag{12}$$

Here, κ is an effective dielectric constant. For the typical electron-electron interaction transition energies, the relevant dielectric constant does not include the difficult-to-model soft-phonon contribution [34], but depends on the dielectric environment on both sides of the relevant heterojunction or surface. For further details on this point see Ref. [45]. In order to take advantage of translational symmetry in the x-y plane, it will be convenient to Fourier transform the Coulomb interaction with respect to the in-plane electron position operators $\boldsymbol{r}_{\perp,i}$:

$$\mathcal{V} = \frac{1}{2A}\sum_{i\neq j}\sum_{\boldsymbol{q}} v_q(z_i-z_j)\, e^{i\boldsymbol{q}\cdot(\boldsymbol{r}_{\perp,i}-\boldsymbol{r}_{\perp,j})}, \tag{13}$$

where $v_q(x) = 2\pi e^2\exp(-q|x|)/(\kappa q)$. We then separate the $\boldsymbol{q}=0$ term in Eq. (13), which can be regularized [29,34,35] by combining it with a remote neutralizing background. This procedure leads, up to an irrelevant constant, to the following Hamiltonian contribution:

$$\mathcal{V}^{\parallel} = -\frac{1}{2A}\sum_{i\neq j}\frac{2\pi e^2}{\kappa}|z_i-z_j|, \tag{14}$$

which we refer to below as the Hartree contribution. Because this term in the Hamiltonian depends only on a small number of macroscopic observables, namely the number of electrons in each layer, its contribution to the ground-state energy is given exactly by the corresponding classical mean-field energy, as discussed in Sec. III B. The remaining portion of the electron-electron interaction,

$$\mathcal{V}^{\perp} = \frac{1}{2A}\sum_{i\neq j}\sum_{\boldsymbol{q}\neq\boldsymbol{0}} v_q(z_i-z_j)\, e^{i\boldsymbol{q}\cdot(\boldsymbol{r}_{\perp,i}-\boldsymbol{r}_{\perp,j})}, \tag{15}$$

gives an energy contribution that is dependent on electronic exchange and correlation effects.

III. VARIATIONAL THEORY FOR THE GROUND-STATE ENERGY

In this section we develop a variational approximation for the ground-state energy that aims to treat interfacial confinement on an equal footing with electrostatic and XC interaction energies. Our strategy is to first assign confinement wave functions to each t_{2g} subband, to then use a two-dimensional random-phase (GW) approximation to account for exchange and correlation with a fixed confinement-wave-function constraint, and finally to optimize the confinement wave functions by minimizing the total energy including electrostatic energies and confinement-direction hopping. The orbital-dependent subband wave functions can be expanded in the form

$$|\psi_{\alpha\sigma}\rangle = \sum_{R_z=1}^{N_l}\eta_{R_z}^{\alpha\sigma}\,|R_z\,\alpha\,\sigma\rangle, \tag{16}$$

where $|R_z\,\alpha\,\sigma\rangle$ is a single-particle confinement direction lattice state. The single-particle Hilbert space is constructed as a direct product of the $|R_z\,\alpha\,\sigma\rangle$ space and two-dimensional momentum space, $|\psi_{\boldsymbol{k}\alpha\sigma}\rangle = |\boldsymbol{k}\rangle\otimes|\psi_{\alpha\sigma}\rangle$. In Sec. III A we derive an expression for the contribution to the ground-state energy from the single-particle and interaction terms that are sensitive to planar spatial correlations: $\mathcal{H}^{\perp} = \mathcal{T}^{\perp} + \mathcal{V}^{\perp}$ (see below). Because the number of electrons in each orbital is a good quantum number, the energy can be expressed as a function of the subband wave-function spinors, $\boldsymbol{\eta}^{\alpha\sigma}$, and the electron density associated with each spin-resolved orbital, $n_{\alpha\sigma}$. In Sec. III B we derive an equation for the wave functions attached to each spin-resolved band that is based on a total-energy minimization principle. Finally, in Sec. III C we describe the self-consistent solution of this equation. Using this procedure we can determine the distribution of density amongst the spin-resolved bands, allowing for the possibility of spontaneous orbital and spin order.

A. Two-dimensional electron gas exchange and correlation

In this section we will apply the random phase approximation (RPA) [29] to a 2DEG Hamiltonian constructed by fixing confinement-direction subband wave functions:

$$\mathcal{H}^{\perp} = \sum_{\alpha\sigma} c^{\dagger}_{\boldsymbol{k}\alpha\sigma} h^{\perp}_{\alpha}(\boldsymbol{k}) c_{\boldsymbol{k}\alpha\sigma} + \frac{1}{2A}\sum_{\boldsymbol{q}\neq 0}\sum_{\substack{\boldsymbol{k}\boldsymbol{k}'\\ \alpha\alpha'\\ \sigma\sigma'}} V_{\alpha\sigma,\alpha'\sigma'}(q)\, c^{\dagger}_{\boldsymbol{k}+\boldsymbol{q}\alpha\sigma} c^{\dagger}_{\boldsymbol{k}'-\boldsymbol{q}\alpha'\sigma'} c_{\boldsymbol{k}'\alpha'\sigma'} c_{\boldsymbol{k}\alpha\sigma}. \tag{17}$$

$\mathcal{H}^{\perp}$ accounts fully for lateral hopping and for the component of Coulomb interactions sensitive to the electron coordinates perpendicular to the confinement direction. It is simply the second-quantization version of Eq. (15) combined with Eq. (9). The dispersion of the bands retained in our model is given in Eq. (8) and plotted in Fig. 1. The orbital- and spin-dependent

effective interaction in Eq. (17) is constructed by attaching the appropriate subband wave function to each orbital and averaging over the confinement direction

$$V_{\alpha\sigma,\alpha'\sigma'}(q) = \sum_{R_{z1},R_{z2}} \left|\eta^{\alpha\sigma}_{R_{z1}}\right|^2 \frac{2\pi e^2 e^{-q|R_{z1}-R_{z2}|}}{\kappa q} \left|\eta^{\alpha'\sigma'}_{R_{z2}}\right|^2. \quad (18)$$

The subband and spin indices in Eq. (18) account for the fact that the Coulomb interaction between an electron in the spin-resolved subband labeled by (α,σ) and an electron in (α',σ') depends on the spatial profile of the respective confinement wave functions. This should not be confused with the more general feature that the bare Coulomb interaction does not allow for any particular electron to scatter between different spin-resolved bands; in the language of Feynman diagrams this is often described by saying that the bare Coulomb interaction vertices are diagonal in the spin and band indices. In the numerical calculations for the t_{2g} 2DEG presented in Sec. IV we limit our consideration to wave functions that depend only on orbital, i.e., $\boldsymbol{\eta}^{\alpha\sigma} \to \boldsymbol{\eta}^{\alpha}$, allowing the spin indices (σ,σ') in Eq. (18) to be dropped. The ground-state energy of the 2DEG Hamiltonian in Eq. (17) has kinetic energy $E^{\perp}_{\mathrm{K}}$, exchange energy $E^{\perp}_{\mathrm{X}}$, and correlation energy $E^{\perp}_{\mathrm{C}}$ contributions that depend on a set of densities that specify the occupation of each spin-resolved band, $\{n_{\alpha\sigma}\}$. The exchange and correlation energies also depend on the set of transverse subband wave functions through the expansion coefficients, $\{\boldsymbol{\eta}^{\alpha\sigma}\}$ defined in Eq. (16). Here and throughout the remainder of this paper we use the convention

$$\{x_{\alpha\sigma}\} \equiv \{x_{xy\uparrow},x_{xy\downarrow},x_{yz\uparrow},x_{yz\downarrow},x_{xz\uparrow},x_{xz\downarrow}\} \quad (19)$$

to express sets of variables that depend on band α and spin σ quantum numbers.

The kinetic energy contribution to the ground-state energy of Eq. (17) is simply the sum of contributions from each occupied spin-resolved band, i.e.,

$$E^{\perp}_{\mathrm{K}} = \sum_{\alpha\sigma} E^{\alpha\sigma}_{\mathrm{K}}. \quad (20)$$

For each spin-resolved isotropic xy band

$$E^{\alpha\sigma}_{\mathrm{K}} = \frac{\pi\hbar^2 A n^2_{\alpha\sigma}}{m_{\mathrm{L}}}, \quad (21)$$

and for each spin-resolved elliptical xz and yz band

$$E^{\alpha\sigma}_{\mathrm{K}} = \frac{\pi\hbar^2 A n^2_{\alpha\sigma}}{m_{\mathrm{DOS}}}, \quad (22)$$

where A is the 2D sample area and we have defined the density-of-states mass $m_{\mathrm{DOS}} = \sqrt{m_{\mathrm{L}} m_{\mathrm{H}}}$. The offset between the xz and yz band-edge energy and the xy band-edge energy is accounted for in the analysis of $\mathcal{H}^{\parallel}$ presented in Sec. III B.

The exchange energy is given by first-order perturbation theory [29]. Since the Coulomb interaction vertices are diagonal in band index, the total exchange energy is given by the sum of independent contributions from each occupied band

$$E^{\perp}_{\mathrm{X}} = \sum_{\alpha\sigma} E^{\alpha\sigma}_{\mathrm{X}}. \quad (23)$$

The exchange energy of electrons in band α and with spin σ is given by

$$E^{\alpha\sigma}_{\mathrm{X}} = -\frac{1}{2A} \sum_{\boldsymbol{k}} n^{(\mathrm{F})}_{\alpha\sigma}(\boldsymbol{k}) \sum_{q\neq 0} V_{\alpha\sigma,\alpha\sigma}(q) n^{(\mathrm{F})}_{\alpha\sigma}(\boldsymbol{k}+\boldsymbol{q}), \quad (24)$$

where $n^{(\mathrm{F})}_{\alpha\sigma}(\boldsymbol{k})$ is the usual Fermi-Dirac distribution function. At zero temperature the integral over $\boldsymbol{k}$ can be performed analytically and the remaining two-dimensional integral over $\boldsymbol{q}$ can be evaluated numerically:

$$E^{\alpha\sigma}_{\mathrm{X}} = -\frac{A}{8\pi^2} \int_0^{\infty} q\, dq \int_0^{2\pi} d\phi \left[\sum_{R_{z1},R_{z2}} \left|\eta^{\alpha\sigma}_{R_{z1}}\right|^2 \frac{2\pi e^2 e^{-qF(\zeta,\phi)|R_{z1}-R_{z2}|}}{\kappa q F(\zeta,\phi)} \left|\eta^{\alpha\sigma}_{R_{z2}}\right|^2 \right] \Theta\left(\sqrt{4\pi n_{\alpha\sigma}} - \frac{q}{2}\right)$$
$$\times \left[n_{\alpha\sigma} - \frac{q}{4\pi^2} \sqrt{4\pi n_{\alpha\sigma} - \left(\frac{q}{2}\right)^2} - \frac{2}{\pi} \arcsin\left(\frac{q}{4\sqrt{\pi n_{\alpha\sigma}}}\right) \right], \quad (25)$$

where $\Theta(x)$ is the Heaviside step function and we have defined

$$F(\zeta,\phi) = \sqrt{\zeta^{-1/2}\cos^2(\phi) + \zeta^{1/2}\sin^2(\phi)}. \quad (26)$$

The parameter $\zeta = m_{\mathrm{H}}/m_{\mathrm{L}}$ in Eq. (25) describes the degree of band anisotropy present in the xz and yz bands. Equation (25) applies to the isotropic xy bands after setting ζ to one, in which case the integral over ϕ becomes trivial.

In the numerical calculations presented in Sec. IV we specifically consider thin films of $SrTiO_3$. Throughout this paper we define the "thin-film limit" quantitatively via the condition $N_l a\sqrt{n/g} \ll 1$, where $\sqrt{n/g}$ is an approximation for the 2D Fermi wave vector of each of the $g = 6$ spin-resolved bands in our t_{2g} 2DEG model and $N_l a$ is the quantum well thickness (i.e., the maximum distance separating any two electrons in the z direction). Qualitatively this limit describes the case when the typical interelectron distance which is perpendicular to the confinement direction, $|\boldsymbol{r}_{\perp,i} - \boldsymbol{r}_{\perp,j}|$, is much greater than the interelectron distance parallel to the confinement direction, $|z_i - z_j|$, and the latter can be neglected. In this limit the Coulomb interaction loses its orbital dependence, and we therefore replace $V_{\alpha\sigma,\alpha\sigma}(q)$ with $v_q \equiv 2\pi e^2/(\kappa q)$. Subsequently, Eq. (25) for the exchange energy of a single spin-resolved band can be evaluated analytically

$$E^{\alpha\sigma}_{\mathrm{X}} = -\frac{16 e^2 n^{3/2}_{\alpha\sigma} A}{3\pi^{3/2}\kappa} \zeta^{1/4}\, \mathrm{K}(1-\zeta), \quad (27)$$

where $\mathrm{K}(x)$ is the complete elliptic integral of the first kind. Equation (27) applies to both the elliptical xz and yz bands and, by setting $\zeta \to 1$, also to the circular xy band.

We note that the exchange energy is *always negative*, that the exchange interaction acts only between electrons in the same spin and orbitally resolved band, and that the dependence of exchange energy on density in a single band is superlinear. It follows that exchange favors states in which electrons occupy fewer bands. This is the physical mechanism for the type of ferromagnetism envisioned by Bloch [15]. In 2DEGs where different bands have different orbital content (e.g., xy, yz, or xz), the exchange interaction can lead to orbitally-ordered states, as well as spin-ordered states. We discuss these types of instabilities in detail in Sec. IV. It follows from Eq. (27) that the exchange energy is weakly reduced by band anisotropy. This property works against exchange-driven spontaneous symmetry breaking in $SrTiO_3$ 2DEGs.

To evaluate the correlation energy we follow the familiar procedure [29] of combining coupling-constant-integration with the fluctuation-dissipation theorem. This method begins by considering the coupling constant of our Hamiltonian (i.e., the electron's charge) as a tunable parameter: We replace $-e$ with $-e\sqrt{\lambda}$ and allow λ to vary between zero and one. The ground-state wave function $\Psi(\lambda)$ and total ground-state energy $E(\lambda)$ both evolve as λ is varied. At any particular value of λ, the contribution to the total ground-state energy from the coupling-constant-rescaled Hamiltonian in Eq. (17) is found by taking the expectation value

$$E^{\perp}(\lambda) = \langle\Psi(\lambda)|\mathcal{H}^{\perp}(\lambda)|\Psi(\lambda)\rangle = \langle\mathcal{T}^{\perp}\rangle_{\lambda} + \langle\mathcal{V}^{\perp}(\lambda)\rangle_{\lambda}. \quad (28)$$

After taking the derivative with respect to λ and using the Hellman-Feynman theorem this becomes

$$\frac{dE^{\perp}(\lambda)}{d\lambda} = \frac{1}{\lambda}\langle\mathcal{V}^{\perp}(\lambda)\rangle_{\lambda}. \quad (29)$$

The XC energy is then obtained by integrating over the coupling constant

$$E^{\perp}_{\rm XC} \equiv E^{\perp}(1) - E^{\perp}(0) = \int_0^1 \frac{d\lambda}{\lambda}\langle\mathcal{V}^{\perp}(\lambda)\rangle_{\lambda}. \quad (30)$$

The instantaneous structure factor [29] describes correlations between density fluctuations at wave vector $-\boldsymbol{q}$ in band (α,σ), and density fluctuations at wave vector $+\boldsymbol{q}$ in band (α',σ'), and is defined by

$$S^{(\lambda)}_{\alpha\sigma,\alpha'\sigma'}(\boldsymbol{q}) = \left\langle n^{\alpha\sigma}_{-\boldsymbol{q}}\, n^{\alpha'\sigma'}_{\boldsymbol{q}}\right\rangle_{\lambda}/N, \quad (31)$$

where $n^{\alpha\sigma}_{-\boldsymbol{q}} = \sum_{\boldsymbol{k}} c^{\dagger}_{\boldsymbol{k}+\boldsymbol{q}\alpha\sigma} c_{\boldsymbol{k}\alpha\sigma}$ and N is the total number of electrons. Equation (30) can then be written

$$E^{\perp}_{\rm XC} = \frac{1}{2A}\int_0^1 \frac{d\lambda}{\lambda}\sum_{\boldsymbol{q}\neq 0}\sum_{\substack{\alpha\alpha'\\ \sigma\sigma'}} V^{(\lambda)}_{\alpha\sigma,\alpha'\sigma'}(q) \times\left[N S^{(\lambda)}_{\alpha\sigma,\alpha'\sigma'}(\boldsymbol{q}) - \delta_{\alpha\alpha'}\delta_{\sigma\sigma'}N_{\alpha\sigma}\right], \quad (32)$$

where $N_{\alpha\sigma}$ is the number of electrons in the spin-resolved band labeled by (α,σ), and $V^{(\lambda)}_{\alpha\sigma,\alpha'\sigma'}$ is given by Eq. (18) after replacing $-e$ with $-e\sqrt{\lambda}$. Next we make use of the fluctuation-dissipation theorem [29] relating the instantaneous structure factor to the density-response function

$$S^{(\lambda)}_{\alpha\sigma,\alpha'\sigma'}(\boldsymbol{q}) = -\frac{2\hbar}{n\pi}\int_0^{\infty}\chi^{(\lambda)}_{\alpha\sigma,\alpha'\sigma'}(\boldsymbol{q},i\omega)\,d\omega. \quad (33)$$

The density-response function, $\chi^{(\lambda)}_{\alpha\sigma,\alpha'\sigma'}(\boldsymbol{q},i\omega)$, is the proportionality factor between the change in electron density at $-\boldsymbol{q}$ in the band labeled by (α,σ), when an arbitrarily weak perturbation couples to the density at $\boldsymbol{q}$ in the band labeled by (α',σ') [29]. We have analytically continued the integration path to the complex frequency axis in Eq. (33) to avoid plasmon poles. We can now write the XC energy as

$$E^{\perp}_{\rm XC} = \frac{1}{2A}\int_0^1 \frac{d\lambda}{\lambda}\sum_{\boldsymbol{q}\neq 0}\sum_{\substack{\alpha\alpha'\\ \sigma\sigma'}} V^{(\lambda)}_{\alpha\sigma,\alpha'\sigma'}(q) \times\left[-\frac{2\hbar A}{\pi}\int_0^{\infty}\chi^{(\lambda)}_{\alpha\sigma,\alpha'\sigma'}(\boldsymbol{q},i\omega)\,d\omega - \delta_{\alpha\alpha'}\delta_{\sigma\sigma'}N_{\alpha\sigma}\right]. \quad (34)$$

Since the exchange energy is equivalent to first-order perturbation theory in homogeneous electron gases, it is clear that we can obtain an alternative expression for the exchange energy by replacing the full density-response function, $\chi^{(\lambda)}_{\alpha\sigma,\alpha'\sigma'}(\boldsymbol{q},i\omega)$, with the noninteracting density-response function, $\chi^{(0)}_{\alpha\sigma,\alpha'\sigma'}(\boldsymbol{q},i\omega)$. Note that the noninteracting density-response function is diagonal in the combined spin-band index (α,σ), i.e., $\chi^{(0)}_{\alpha\sigma,\alpha'\sigma'}(\boldsymbol{q},i\omega) = \delta_{\alpha\alpha'}\delta_{\sigma\sigma'}\chi^{(0)}_{\alpha\sigma}(\boldsymbol{q},i\omega)$. We can subtract the coupling-constant-integration expression for the exchange energy from Eq. (34) to obtain the correlation energy

$$E^{\perp}_{\rm C} = \frac{-\hbar}{\pi}\int_0^{\infty} d\omega\int_0^1 \frac{d\lambda}{\lambda}\sum_{\boldsymbol{q}\neq 0}\sum_{\substack{\alpha\alpha'\\ \sigma\sigma'}} V^{(\lambda)}_{\alpha\sigma,\alpha'\sigma'}(q) \times\left[\chi^{(\lambda)}_{\alpha\sigma,\alpha'\sigma'}(\boldsymbol{q},i\omega) - \chi^{(0)}_{\alpha\sigma,\alpha'\sigma'}(\boldsymbol{q},i\omega)\right]. \quad (35)$$

It is, in fact, necessary to remove the exchange-energy contribution from the coupling-constant formulation of the XC energy in order to obtain a convergent frequency integral.

The density-response functions appearing in Eq. (35) form a matrix, $\boldsymbol{\chi}^{(\lambda)}(\boldsymbol{q},\omega)$, with rows labeled by (α,σ) and columns labeled by (α',σ'). In the RPA, the density-response matrix is related to the diagonal matrix of noninteracting density-response functions $\boldsymbol{\chi}^{(0)}(\boldsymbol{q},\omega) \equiv \mathrm{diag}(\chi^{(0)}_{\alpha_1\uparrow}(\boldsymbol{q},\omega), \chi^{(0)}_{\alpha_1\downarrow}(\boldsymbol{q},\omega), \chi^{(0)}_{\alpha_2\uparrow}(\boldsymbol{q},\omega), \chi^{(0)}_{\alpha_2\downarrow}(\boldsymbol{q},\omega), \dots)$ via

$$[\boldsymbol{\chi}^{(\lambda)}(\boldsymbol{q},i\omega)]^{-1} = [\boldsymbol{\chi}^{(0)}(\boldsymbol{q},i\omega)]^{-1} - \boldsymbol{V}^{(\lambda)}(\boldsymbol{q}), \quad (36)$$

where the elements of the matrix $\boldsymbol{V}^{(\lambda)}(\boldsymbol{q})$ are given by Eq. (18) after replacing $-e$ with $-e\sqrt{\lambda}$. Analytic expressions for $\mathrm{Re}\,\chi^{(0)}_{xy\sigma}(\boldsymbol{q},i\omega)$ and $\mathrm{Im}\,\chi^{(0)}_{xy\sigma}(\boldsymbol{q},i\omega)$ for the isotropic 2D band case can be found, for example, in Ref. [29]. The subband wave functions, $\boldsymbol{\eta}^{\alpha\sigma}$, do not change these functions from the formulas for a perfectly two-dimensional system. The analytic expressions for the elliptical-band response functions $\chi^{(0)}_{xz\sigma}(\boldsymbol{q},i\omega)$ $[\chi^{(0)}_{yz\sigma}(\boldsymbol{q},i\omega)]$ can be easily identified by rescaling momenta, $k_x \to k_x\sqrt{m_{\rm L}/m_{\rm DOS}}$ and $k_y \to k_y\sqrt{m_{\rm H}/m_{\rm DOS}}$ $[k_x \to k_x\sqrt{m_{\rm H}/m_{\rm DOS}}$ and $k_y \to k_y\sqrt{m_{\rm L}/m_{\rm DOS}}]$ in Eq. (8). Since this rescaling maps the elliptical band onto a circular band, the elliptical band density-response functions $\chi^{(0)}_{xz\sigma}(\boldsymbol{q},i\omega)$ and $\chi^{(0)}_{yz\sigma}(\boldsymbol{q},i\omega)$ can be written in terms of $\chi^{(0)}_{xy\sigma}(\boldsymbol{q},i\omega)$:

$$\chi^{(0)}_{xz\sigma}(\boldsymbol{q},i\omega) = \chi^{(0)}_{xy\sigma}(q',i\omega;m_{\rm DOS})\big|_{q'\to\sqrt{q_x^2\zeta^{1/2}+q_y^2\zeta^{-1/2}}} \quad (37)$$

and

$$\chi^{(0)}_{yz\sigma}(\boldsymbol{q},i\omega) = \chi^{(0)}_{xy\sigma}(q',i\omega;m_{\rm DOS})\big|_{q'\to\sqrt{q_x^2\zeta^{-1/2}+q_y^2\zeta^{1/2}}}, \quad (38)$$

where we have again defined $\zeta = m_{\rm H}/m_{\rm L}$. Equations (35) and (36) combine to give a general expression for the RPA correlation energy which can be applied to 2DEGs with an arbitrary number of subbands. When the number of bands is sufficiently small, Eq. (36) can be inverted analytically and the integral over the coupling-constant λ can be performed by hand. Furthermore, if each band is isotropic then the noninteracting density-response functions depend only on $|\boldsymbol{q}|$ and the integral over wave-vector orientation angle is trivial.

In applying the coupling-constant integration algorithm to the t_{2g} model for $SrTiO_3$, we assume that all electrons in the elliptical xz and yz bands can be described by a single transverse wave function, $\boldsymbol{\eta}^{\rm E}$, while all electrons in the circular xy band can be described by a second transverse wave function, $\boldsymbol{\eta}^{\rm C}$. This approximation is motivated by Eq. (6), which says that electrons in the elliptical bands hop between layers in the $\hat{z}$ direction with amplitude t, while electrons in the circular band hop with amplitude t'. There are then only three distinct interactions contained in Eq. (18), i.e., $V_{\rm C,C} = V_{xy\sigma,xy\sigma'}$, $V_{\rm E,E} = V_{xz\sigma,xz\sigma'} = V_{yz\sigma,yz\sigma'} = V_{xz\sigma,yz\sigma'} = V_{yz\sigma,xz\sigma'}$, and $V_{\rm C,E} = V_{\rm E,C} = V_{xy\sigma,xz\sigma'} = V_{xy\sigma,yz\sigma'} = V_{xz\sigma,xy\sigma'} = V_{yz\sigma,xy\sigma'}$ where we have omitted the q dependence of the interactions for brevity. Since there are only two independent components, Eq. (36) becomes

$$[\boldsymbol{\chi}^{(\lambda)}(\boldsymbol{q},i\omega)]^{-1} = \begin{pmatrix} \left(\chi^{(0)}_{\rm C}\right)^{-1} & 0 \\ 0 & \left(\chi^{(0)}_{\rm E}\right)^{-1} \end{pmatrix} - \begin{pmatrix} V^{(\lambda)}_{\rm C,C} & V^{(\lambda)}_{\rm C,E} \\ V^{(\lambda)}_{\rm E,C} & V^{(\lambda)}_{\rm E,E} \end{pmatrix}. \quad (39)$$

Here, $\chi^{(0)}_{\rm C}(\boldsymbol{q},i\omega)$ is the density response function of the circular bands,

$$\chi^{(0)}_{\rm C}(\boldsymbol{q},i\omega) = \sum_{\sigma} \chi^{(0)}_{xy\sigma}(\boldsymbol{q},i\omega), \quad (40)$$

and $\chi^{(0)}_{\rm E}(\boldsymbol{q},i\omega)$ is the density response function of the elliptical bands,

$$\chi^{(0)}_{\rm E}(\boldsymbol{q},i\omega) = \sum_{\sigma}\sum_{\alpha=xz,yz} \chi^{(0)}_{\alpha\sigma}(\boldsymbol{q},i\omega). \quad (41)$$

Finally, as in the calculation of the exchange energy presented above, we consider the thin-film limit in which the Coulomb-interaction entering the RPA correlation energy loses its orbital dependence, and we can replace $V_{\alpha\sigma,\alpha'\sigma'}(q)$ with v_q. Equation (39) simplifies to a single-component expression

$$\frac{1}{\chi^{(\lambda)}(\boldsymbol{q},\omega)} = \frac{1}{\chi^{(0)}(\boldsymbol{q},\omega)} - v_q^{(\lambda)}, \quad (42)$$

where we define $\chi^{(0)}(\boldsymbol{q},\omega) = \sum_{\alpha\sigma}\chi^{(0)}_{\alpha\sigma}(\boldsymbol{q},\omega)$. In this same limit Eq. (35) reduces to

$$E^{\perp}_{\rm C} = \frac{-\hbar}{\pi}\int_0^{\infty} d\omega \int_0^1 \frac{d\lambda}{\lambda} \sum_{\boldsymbol{q}\neq 0} v_q[\chi^{(\lambda)}(\boldsymbol{q},i\omega) - \chi^{(0)}(\boldsymbol{q},i\omega)], \quad (43)$$

which after carrying out the integration over the coupling constant gives

$$E^{\perp}_{\rm C} = \frac{-\hbar}{\pi}\int_0^{\infty} d\omega \sum_{\boldsymbol{q}\neq 0}[v_q\,\chi^{(0)}(\boldsymbol{q},i\omega) + \ln(1 - v_q\,\chi^{(0)}(\boldsymbol{q},i\omega))]. \quad (44)$$

As explained in more detail in Appendix A, we find that the (always negative) correlation energy per electron is decreased in magnitude by increasing the band anisotropy. Furthermore, the correlation energy is largest in magnitude when the electron density is distributed equally amongst all of the spin-resolved bands. This property implies that the correlation energy works against the type of spontaneous symmetry breaking favored by exchange. We discuss this competition in Sec. IV, but first must account for the contribution to the ground-state energy from the $q = 0$ electron-electron interaction term (i.e., the Hartree potential), the electrostatic external potential, and from hopping between layers.

In this section we have obtained expressions for the contribution to the total ground-state energy from terms in the t_{2g} 2DEG Hamiltonian which are sensitive to electron positions perpendicular to the confinement direction

$$E^{\perp} = E^{\perp}_{\rm K} + E^{\perp}_{\rm X} + E^{\perp}_{\rm C}. \quad (45)$$

In the next section we will give expressions for the total ground-state energy of the t_{2g} 2DEG Hamiltonian by combining Eq. (45) with the expectation value of the terms which are sensitive to electron positions parallel to the confinement direction. Before we do this, we pause to note that neither our thin-film approximation, $N_l a\sqrt{n/g} \ll 1$, nor our restriction to only two distinct transverse wave functions, $(\boldsymbol{\eta}^{\rm C},\boldsymbol{\eta}^{\rm E})$, are critical to the applicability of the variational theory.

B. Total energy

Next we calculate the contribution to the total ground-state energy from terms in the t_{2g} 2DEG Hamiltonian that are sensitive to the electron position in the direction parallel to the confinement direction, $\mathcal{H}^{\parallel} = \mathcal{T}^{\parallel} + \mathcal{V}^{\parallel} + \mathcal{V}^{\parallel}_{\rm ext}$. This is obtained by taking the expectation value of $\mathcal{H}^{\parallel}$ in the many-body state defined by

$$\left\langle \Psi_{\{n_{\alpha\sigma},\boldsymbol{\eta}^{\alpha\sigma}\}}\middle|\mathcal{H}^{\perp}\middle|\Psi_{\{n_{\alpha\sigma},\boldsymbol{\eta}^{\alpha\sigma}\}}\right\rangle = E^{\perp}. \quad (46)$$

Although $E^{\perp}$ was not calculated in the previous section by appealing to an explicit many-body wave function, the appropriate N-electron wave function can always be written as a linear combination of Slater determinants of single-particle states $|\psi_{\boldsymbol{k}\alpha\sigma}\rangle$:

$$\left|\Psi_{\{n_{\alpha\sigma},\boldsymbol{\eta}^{\alpha\sigma}\}}\right\rangle = \sum_i c_i \left\{\sum_{\rm P}(-1)^{\rm P}\hat{\rm P}\left[\prod_{j=1}^{\rm N}\left|\psi_{\boldsymbol{k}_j\alpha_j\sigma_j}\right\rangle\right]\right\}, \quad (47)$$

where $\hat{\rm P}$ is the permutation operator, P is the number of permutations in each term, and we are summing over all permutations of the single-particle state labels amongst the N electrons. Here, c_i is a complex coefficient and the index i runs over all Slater determinants with a fixed number of electrons in each spin-resolved band and fixed transverse wave fuctions;

we choose the sets $\{n_{\alpha\sigma}\}$ and $\{\boldsymbol{\eta}^{\alpha\sigma}\}$ as good quantum numbers of our many-body variational wave function $|\Psi_{\{n_{\alpha\sigma},\boldsymbol{\eta}^{\alpha\sigma}\}}\rangle$.

The first contribution to $E^{\parallel}$ is from interlayer hopping described by Eq. (6). Taking the expectation value of $\mathcal{T}^{\parallel}$ we find that

$$E^{\parallel}_{\rm K} = A\sum_{\alpha\sigma} n_{\alpha\sigma}(\boldsymbol{\eta}^{\alpha\sigma\dagger}\cdot\boldsymbol{t}^{\alpha}\cdot\boldsymbol{\eta}^{\alpha\sigma}), \tag{48}$$

where $\boldsymbol{t}^{xz} = \boldsymbol{t}^{yz} = -t\,\delta_{R_z,R_z\pm a} + 2(t-t')\,\delta_{R_z,R'_z}$ and $\boldsymbol{t}^{xy} = -t'\,\delta_{R_z,R_z\pm a}$ are $N_l \times N_l$ matrices in layer index. The diagonal contribution $2(t-t')$ to $\boldsymbol{t}^{xz}$ and $\boldsymbol{t}^{yz}$ accounts for the energy offset between the band edge of the elliptical xz and yz bands and the circular xy band when confined to a single TiO_2 layer (see Fig. 1). This expression is independent of the correlations among transverse degrees of freedom, approximated above using the RPA. Similarly, the Hartree energy can be obtained by taking the expectation value of the portion of the Coulomb interaction sensitive to electron positions along the confinement direction, $\mathcal{V}^{\parallel}$:

$$\begin{aligned} E^{\parallel}_{\rm H} &= A\sum_{\alpha\sigma} n_{\alpha\sigma}\left(\boldsymbol{\eta}^{\alpha\sigma\dagger}\cdot\boldsymbol{V}_{\rm H}\cdot\boldsymbol{\eta}^{\alpha\sigma}\right) \\ &= -A\frac{\pi e^2}{\kappa}\sum_{R_z,R'_z} n_{R_z}\,|R_z - R'_z|\,n_{R'_z}, \end{aligned} \tag{49}$$

where n_{R_z} is the total electron density in layer R_z. The matrix $\boldsymbol{V}_{\rm H}$ entering Eq. (49) is diagonal in TiO_2 layer index, with elements given by

$$[\boldsymbol{V}_{\rm H}]_{R_z,R'_z} = -\delta_{R_z,R'_z}\left(\frac{\pi e^2}{\kappa}\right)\sum_{R''_z}|R_z - R''_z|\sum_{\alpha\sigma} n_{\alpha\sigma}\left|\eta^{\alpha\sigma}_{R''_z}\right|^2. \tag{50}$$

For definiteness, we will assume in this paper the common case in which there is only one electrostatic gate (which we place at $z=0$) with total charge $+e\,n = +e\sum_{\alpha\sigma} n_{\alpha\sigma}$ (see Fig. 1). The electronic energy from the external gate's confinement potential is then

$$E^{\parallel}_{\rm ext} = A\sum_{\alpha\sigma} n_{\alpha\sigma}(\boldsymbol{\eta}^{\alpha\sigma\dagger}\cdot\boldsymbol{V}_{\rm ext}\cdot\boldsymbol{\eta}^{\alpha\sigma}), \tag{51}$$

where $\boldsymbol{V}_{\rm ext}$ is also a diagonal matrix in TiO_2 layer index, with matrix elements given by

$$[\boldsymbol{V}_{\rm ext}]_{R_z,R'_z} = \left(\frac{2\pi e^2 n R_z}{\kappa}\right)\delta_{R_z,R'_z}. \tag{52}$$

Combining terms, we write the contribution from the parallel part of the Hamiltonian to the total ground-state energy as

$$E^{\parallel} = E^{\parallel}_{\rm K} + E^{\parallel}_{\rm H} + E^{\parallel}_{\rm ext}. \tag{53}$$

Notice that since each term in $\mathcal{H}^{\perp}$ depends only on a small number of macroscopic observables (e.g., the density in each layer and/or the density in each spin-resolved band), which are completely determined from the good quantum numbers of our variational wave function Eq. (47), each term's contribution to the ground-state energy is given exactly by the corresponding classical mean-field energy.

When $E^{\parallel}$ is combined with the contributions to the ground-state energy from the perpendicular part of the Hamiltonian, we obtain the total ground-state energy as a functional of the density in each spin-resolved band and the transverse subband wave-function spinors:

$$E[\{n_{\alpha\sigma},\boldsymbol{\eta}^{\alpha\sigma}\}] = E^{\parallel} + E^{\perp}. \tag{54}$$

C. Minimizing the total energy

To solve for the ground-state values of $\{n_{\alpha\sigma}\}$ and $\{\boldsymbol{\eta}^{\alpha\sigma}\}$, we minimize the energy functional in Eq. (54) subject to the constraint equations

$$\begin{aligned} \sum_{\alpha\sigma} n_{\alpha\sigma} &= n \\ \sum_{R_z}\left|\eta^{\alpha\sigma}_{R_z}\right|^2 &= 1. \end{aligned} \tag{55}$$

The second equation is applied for each α and σ. For these constraints we introduce Lagrange multipliers, μ and $\{\nu_{\alpha\sigma}\}$, respectively. Minimization of the total energy functional with respect to each particular $n_{\alpha\sigma}$ yields an equation

$$\mu^{\perp}_{\alpha\sigma} + \boldsymbol{\eta}^{\alpha\sigma\dagger}\cdot(\boldsymbol{t}^{\alpha} + \boldsymbol{V}_{\rm H} + \boldsymbol{V}_{\rm ext})\cdot\boldsymbol{\eta}^{\alpha\sigma} = \mu, \tag{56}$$

where we have defined $\mu^{\perp}_{\alpha\sigma} = A^{-1}\,dE^{\perp}/dn_{\alpha\sigma}$. In obtaining the results presented in Sec. IV, we have evaluated $\mu^{\perp}_{\alpha\sigma}$ numerically by combining the above expressions for $E^{\perp}$ with finite difference formulas. Minimization of the total energy functional with respect to each component of the spinor $\boldsymbol{\eta}^{\alpha\sigma\dagger}$ yields an eigenvalue equation

$$(\boldsymbol{X} + \boldsymbol{Y}^{\alpha\sigma} + \boldsymbol{t}^{\alpha\sigma} + \boldsymbol{V}_{\rm H} + \boldsymbol{V}_{\rm ext})\cdot\boldsymbol{\eta}^{\alpha\sigma} = \left(\frac{\nu_{\alpha\sigma}}{A\,n_{\alpha\sigma}}\right)\boldsymbol{\eta}^{\alpha\sigma} \tag{57}$$

for each value of α and σ. Here, the diagonal matrices $\boldsymbol{X}$ and $\boldsymbol{Y}^{\alpha\sigma}$ are found from differentiating the correlation energy and exchange energy, respectively, and their matrix elements are given by

$$\begin{aligned} [\boldsymbol{X}]_{R_z,R'_z} = \delta_{R_z,R'_z}\left(\frac{-\hbar}{\pi}\right)\int_0^{\infty} d\omega\int_0^1\frac{d\lambda}{\lambda}\sum_{\boldsymbol{q}\neq 0}\sum_{\substack{\alpha\alpha'\\ \sigma\sigma'}} \\ \times\left(M_{\alpha\sigma,\alpha'\sigma'}(R_z,q)\left\{\chi^{(\lambda)}_{\alpha\sigma,\alpha'\sigma'} - \chi^{(0)}_{\alpha\sigma,\alpha'\sigma'}\right\} + V^{(\lambda)}_{\alpha\sigma,\alpha'\sigma'}(q)\sum_{\substack{\beta\beta'\\ \tau\tau'}}\chi^{(\lambda)}_{\alpha\sigma,\beta\tau}\,M_{\beta\tau,\beta'\tau'}(R_z,q)\,\chi^{(\lambda)}_{\beta'\tau',\alpha'\sigma'}\right) \end{aligned} \tag{58}$$

and

$$[\boldsymbol{Y}^{\alpha\sigma}]_{R_z,R_z'} = \delta_{R_z,R_z'}\left(\frac{-A}{8\pi^2}\right)\int_0^\infty q\,dq\int_0^{2\pi} d\phi\; M_{\alpha\sigma,\alpha\sigma}(R_z,q\,F[\zeta,\phi])\;\Theta\left(\sqrt{4\pi n_{\alpha\sigma}}-\frac{q}{2}\right)$$
$$\times\left[n_{\alpha\sigma}-\frac{q}{4\pi^2}\sqrt{4\pi n_{\alpha\sigma}-\left(\frac{q}{2}\right)^2}-\frac{2}{\pi}\arcsin\left(\frac{q}{4\sqrt{\pi n_{\alpha\sigma}}}\right)\right], \tag{59}$$

where we have defined

$$M_{\alpha\sigma,\alpha'\sigma'}(R_z,q)=\sum_{R_z''}\frac{2\pi e^2 e^{-q|R_z-R_z''|}}{\kappa q}\left(\left|\eta^{\alpha\sigma}_{R_z''}\right|^2+\left|\eta^{\alpha'\sigma'}_{R_z''}\right|^2\right). \tag{60}$$

In Eq. (58) we have omitted the $(\boldsymbol{q},i\omega)$ dependence of the density response functions for brevity. Equations (55)–(57) provide enough independent linear relationships to solve self-consistently for the various densities, $\{n_{\alpha\sigma}\}$, and transverse wave-function spinors $\{\boldsymbol{\eta}^{\alpha\sigma}\}$, introduced in our model.

As already mentioned above, the numerical results we present in Sec. IV have been obtained for thin films of $SrTiO_3$, which we identify by the condition $N_l a\sqrt{n/g}\ll 1$. While this approximation is not essential to our variational approach, by making it we simplify the numerical problem to be solved in this first application of our method in which we study orbital and spin ordering instabilities. Specifically, in the thin-film limit the Coulomb interaction, Eq. (18), loses its orbital dependence and the exchange and correlation energies are no longer directly dependent on the transverse wave-function spinors [see Eqs. (27) and (44)]. As a result the matrices $\boldsymbol{X}$ and $\boldsymbol{Y}^{\alpha\sigma}$ vanish. After also making the approximation that only two distinct transverse wave-function spinors exist, $\boldsymbol{\eta}^{\mathrm{C}}$ and $\boldsymbol{\eta}^{\mathrm{E}}$, the constraints in Eq. (55) can be written as

$$\begin{aligned}\sum_{\beta=\mathrm{E,C}} n_\beta &= n\\ \sum_{R_z}\left|\eta^{\mathrm{C}}_{R_z}\right|^2 &= 1\\ \sum_{R_z}\left|\eta^{\mathrm{E}}_{R_z}\right|^2 &= 1,\end{aligned} \tag{61}$$

and Eqs. (56) and (57) become

$$\mu_\beta^\perp+\boldsymbol{\eta}^\beta\cdot(\boldsymbol{t}^\beta+\boldsymbol{V}_{\mathrm{H}}+\boldsymbol{V}_{\mathrm{ext}})\cdot\boldsymbol{\eta}^\beta=\mu \tag{62}$$

and

$$(\boldsymbol{t}^\beta+\boldsymbol{V}_{\mathrm{H}}+\boldsymbol{V}_{\mathrm{ext}})\cdot\boldsymbol{\eta}^\beta=\left(\frac{\nu_\beta}{A\,n_\beta}\right)\boldsymbol{\eta}^\beta, \tag{63}$$

where $\beta=$ E or C. Equation (62) guarantees that all occupied subbands have the same chemical potential, while Eq. (63) chooses the subband wave function as the eigenvalue of the mean-field Hamiltonian. Appropriate expressions for matrices $\boldsymbol{t}^\beta$ and $\boldsymbol{V}_{\mathrm{H}}$, as well as for $\mu_\beta^\perp$ follow in an obvious manner from the more general definitions in Sec. III B. We note in passing that although the exchange and correlation energies in this approximation are no longer directly dependent on the transverse wave-function spinors, they are still sensitive to confinement effects. For example, the spinors, $\boldsymbol{\eta}^{\mathrm{C}}$ and $\boldsymbol{\eta}^{\mathrm{E}}$ are determined by solving Eq. (63) and are therefore sensitive to the band offset between the xz and yz bands and the xy bands. The band offset obviously influences the equilibrium values of n_β, which in turn affects the values of the exchange and correlation energies defined in Eqs. (27) and (44).

We now outline one method for obtaining the self-consistent solution. The first step in the determination of the densities $(n_{\mathrm{E}},n_{\mathrm{C}})$, and wave functions $(\boldsymbol{\eta}^{\mathrm{E}},\boldsymbol{\eta}^{\mathrm{C}})$, is to make an initial choice for them which satisfies the equations of constraint. In step two, use these to calculate $\boldsymbol{V}_{\mathrm{H}}$, $\mu_{\mathrm{E}}^\perp$, and $\mu_{\mathrm{C}}^\perp$. Equation (62) with $\beta=\mathrm{C}$ can be combined with Eq. (62) with $\beta=\mathrm{E}$ to eliminate μ, and root-finding numerical algorithms can be applied to solve for new values of n_{E} and n_{C}. These values are then used to re-evaluate the Hartree potential $\boldsymbol{V}_{\mathrm{H}}$. Equation (63) is an eigenvalue problem with a real, symmetric, and tridiagonal matrix. It follows that the eigenvalues are real and the eigenvectors can be chosen to have only real components, i.e., $(\boldsymbol{\eta}^\beta)^\dagger=(\boldsymbol{\eta}^\beta)^{\mathrm{T}}$. We solve this eigenvalue problem numerically and select the eigenvectors, $\boldsymbol{\eta}^{\mathrm{E}}$ and $\boldsymbol{\eta}^{\mathrm{C}}$, which correspond to the smallest eigenvalues. These eigenvalues correspond to the band-edge energies of the subbands in our model. We keep the wave functions corresponding to the smallest energy eigenvalues because we are only interested in keeping the lowest subband of each orbital type xy, xz, and yz. We next return to the aforementioned "step two," and repeat until convergence is obtained. Adaptable numerical algorithms exist in the literature [46,47] to assist in solving the eigenvalue problem, finding spline interpolations for the correlation energy, finding roots, and evaluating multidimensional integrals.

After a self-consistent solution has been obtained, the eigenvalues of Eq. (63) give an approximation for the band-edge energies of the bands retained in the t_{2g} 2DEG model. Since our variational theory (just like the Hohenberg-Kohn-Sham formulation of density functional theory) is a ground-state theory, we cannot expect that single-particle energies arising therein will give a perfect description of experimental energies. However, we suspect that they will be an improvement over the LDA because, as discussed in the introduction, our method is sensitive to the electron's orbital symmetry. In Sec. IV we present numerical calculations using the RPA for the matrix of density-response functions $\boldsymbol{\chi}^{(\lambda)}(\boldsymbol{q},i\omega)$. While being exact at high electron density, the RPA neglects vertex corrections which become more important at very low density [48]. Various methods exist for including vertex-correction physics in the matrix of density-response functions (see Ref. [29] and references therein), and we propose that in future calculations the relative success of these approximations [49] can be gauged by comparing the predicted band-edge energy offsets against

those measured directly in angle-resolved photoemission experiments.

IV. SPIN AND ORBITAL ORDER

In this section we present the results of our variational calculation for the ground-state energy as a function of $n_{\rm E}, n_{\rm C}, \boldsymbol{\eta}^{\rm E}$, and $\boldsymbol{\eta}^{\rm C}$. Specifically, we consider *three* types of fully broken symmetry states characterized by the distribution of electrons in the four spin-resolved elliptical bands: spin-ordered (e.g., $n_{xz\uparrow} = n_{yz\uparrow} = n_{\rm E}/2$ and $n_{xz\downarrow} = n_{yz\downarrow} = 0$), orbital-ordered ($n_{xz\uparrow} = n_{xz\downarrow} = n_{\rm E}/2$ and $n_{yz\uparrow} = n_{yz\downarrow} = 0$), and orbital- *and* spin-ordered ($n_{xz\uparrow} = n_{\rm E}$ and $n_{xz\downarrow} = n_{yz\uparrow} = n_{yz\downarrow} = 0$). The fully spin-polarized state of a single-band isotropic 2DEG with Coulomb interactions is known to be energetically favorable compared to a partially spin-polarized state [22,29], which has motivated us to consider only the aforementioned fully spin and/or orbitally polarized states in the oxide 2DEG. In all of these states we keep the density in the isotropic xy band equally distributed amongst the two spin species, $n_{xy\uparrow} = n_{xy\downarrow} = n_{\rm C}/2$. The distribution of electrons in these spontaneously broken symmetry states contrasts with the distribution in the normal phase, where all four spin-resolved elliptical bands are either equally occupied (above some critical density which depends on the thickness of $SrTiO_3$), or all empty. Each broken symmetry state has is own set of $n_{\rm E}, n_{\rm C}, \boldsymbol{\eta}^{\rm E}$, and $\boldsymbol{\eta}^{\rm C}$, which we vary to find the ground-state energy of that phase. By selecting the state with the lowest energy at each value of total 2DEG density n and number of TiO_2 layers N_l, we have constructed the phase diagrams shown in Fig. 2.

Examining Fig. 2(a), we find that spontaneous orbital-order occurs first and is joined by an accompanying spin order as the density is decreased. Several striking features appear here. First, the lower critical density for symmetry breaking decreases as the thickness of $SrTiO_3$ increases. Rather than being an interaction effect, this is caused by a reduction in the intrinsic band-edge offset $2(t - t')$, see, e.g., Fig. 1. Specifically, the elliptical xz and yz bands have a large hopping amplitude parallel to confinement t, and the isotropic xy band has a small hopping amplitude t'. Therefore the xy band is more tightly localized to the interface than the xz and yz bands (a result that is quantitatively contained in the differences between $\boldsymbol{\eta}^{\rm C}$ and $\boldsymbol{\eta}^{\rm E}$, respectively), and the difference in band-edge energies decreases relative to the single-layer value. This mechanism becomes more pronounced as the sample thickness is increased, leading to a smaller effective band-edge offset at each given total density. Accurately capturing the change in band-edge offset as the total density is varied, and perhaps more importantly as density is allowed to shift between the elliptic bands to the circular bands near an instability, is key to finding the correct phase diagram. In the next section we elaborate on the role of correlations in selecting the most energetically favorable broken symmetry state.

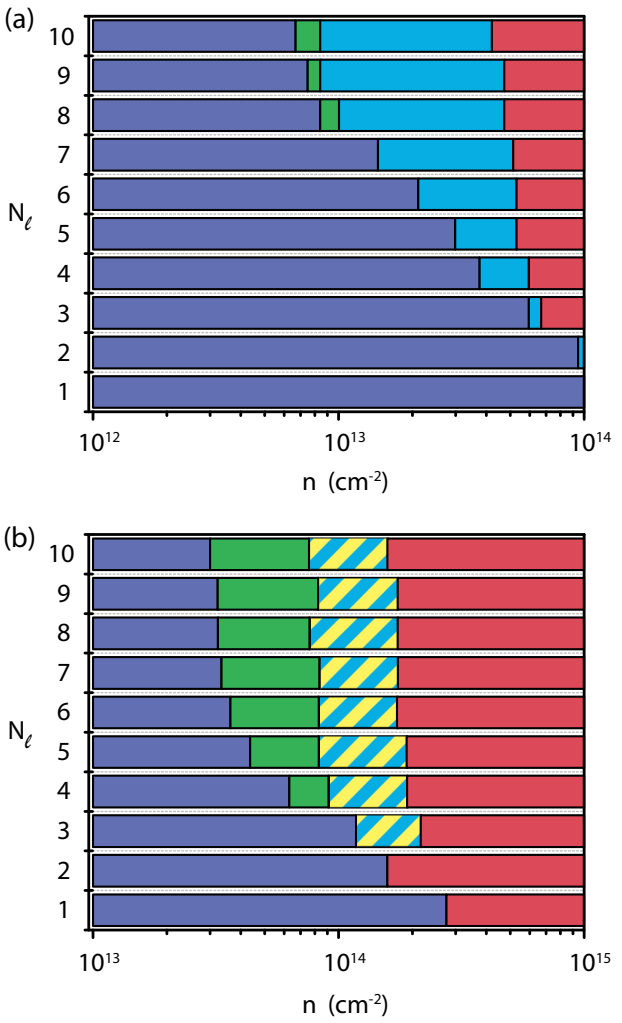

FIG. 2. Phase diagram for the t_{2g} 2DEG model of $SrTiO_3$ plotted for varying total density n and number of TiO_2 layers N_l. In all phases shown there is a finite electron density in the isotropic xy band which is equally distributed between spins. The colors distinguish phases with different distributions of electrons amongst the four spin-resolved elliptical bands ($xz,\uparrow$, $xz,\downarrow$, $yz,\uparrow$, and $yz,\downarrow$). Purple identifies the normal low-density state in which no electrons occupy the elliptical bands. Green identifies a orbital- *and* spin-ordered state in which only one of the spin-resolved elliptical bands contains electrons (e.g., $xz,\uparrow$). Light blue identifies an orbital-ordered state in which only one elliptical band is occupied (e.g., $xz,\uparrow$ and $xz,\downarrow$). Yellow identifies a spin-ordered state in which both elliptical bands have electrons but only of one spin species (e.g., $xz,\uparrow$ and $yz,\uparrow$). Red identifies the normal high-density state in which the density in all four spin-resolved elliptical bands is equal. In panel (a) correlations are included within the RPA. In panel (b) correlations are neglected and only the exchange energy is included. Although the orbital-ordered state is degenerate with the spin-ordered state in (b), correlations prefer an orbital-ordered state and the spin-ordered state is absent in (a).

A. Plasmon-pole approximation: Correlations prefer orbital order

In the isotropic single-band 2DEG, the competition between kinetic and exchange energies qualitatively captures the transition from the normal to the ferromagnetic state. The role of correlations is to lower the critical density for symmetry breaking [29]. Surprisingly, in our model for thin-film $SrTiO_3$ heterojunctions, we find that the correlation energy plays a more qualitative role. More specifically, at the exchange-only

level the spin-ordered state is energetically degenerate with the orbital-ordered state, as shown by the presence of the diagonally-hatched blue and yellow region in Fig. 2(b). The effective exchange interaction only acts between electrons in the same spin-resolved band and therefore the ground-state energy is insensitive to whether the $xz,\uparrow$ and $xz,\downarrow$ bands are occupied, as in a orbital-ordered state, or whether the $xz,\uparrow$ and $yz,\uparrow$ bands are occupied, as in a spin-ordered state; the total exchange energy is given in Eq. (23) and is simply the sum of the exchange energy from each separate spin-resolved band. Once correlations are included, however, our calculations reveal that the system prefers orbital-order to spin-order. Indeed, the orbitally ordered phase (blue) remains in Fig. 2(a), while the spin ordered phase (yellow) is absent.

This result can be understood by applying the *plasmon-pole approximation* (PPA) to the RPA correlation energy. For simplicity we consider a model without the xy band, and only consider the four remaining bands (i.e., $\alpha = xz, yz$ and $\sigma = \uparrow,\downarrow$) of our model. The plasmon frequency of the spin polarized (SP) and orbitally polarized (OP) states is given by the zeros of their respective dielectric functions

$$\epsilon(\boldsymbol{q},\Omega_i) = 1 - v_q \tilde{\chi}_i(\boldsymbol{q},\Omega_i) = 0, \tag{64}$$

where $i =$ OP or SP, and $\tilde{\chi}_i(\boldsymbol{q},\omega)$ is the *proper* density response function of the ith broken symmetry state. In the RPA the proper density response function is given by summing the noninteracting density response function of each occupied spin-resolved band. For the orbital-ordered state

$$\tilde{\chi}_{\rm OP}(\boldsymbol{q},\omega) = \chi^{(0)}_{xz,\uparrow}(\boldsymbol{q},\omega) + \chi^{(0)}_{xz,\downarrow}(\boldsymbol{q},\omega), \tag{65}$$

and for the spin-polarized state

$$\tilde{\chi}_{\rm SP}(\boldsymbol{q},\omega) = \chi^{(0)}_{xz,\uparrow}(\boldsymbol{q},\omega) + \chi^{(0)}_{yz,\uparrow}(\boldsymbol{q},\omega). \tag{66}$$

To make analytic progress we will consider plasmons in the long-wavelength limit (i.e., $q \to 0$ and $\omega > v_{\rm F} q$). The noninteracting density response function of an isotropic band (e.g., the xy band we are currently neglecting) in this limit is [29]

$$\lim_{q\to 0} \chi^{(0)}_{xy\sigma}(q,\omega) = \frac{n_{xy\sigma} q^2}{m_{\rm L}\,\omega^2}. \tag{67}$$

Expressions for the long-wavelength noninteracting density response functions of the elliptical xz and yz bands can be found from Eqs. (37) and (38). After inserting the relevant proper density response function into Eq. (64), we find the plasmon frequency of the spin-ordered and orbital-ordered state is

$$\Omega_{\rm SP} = \sqrt{\frac{v_q n}{2\bar{m}}}\, q \tag{68}$$

and

$$\Omega_{\rm OP} = \sqrt{\frac{v_q n}{m_{\rm DOS}}}\sqrt{\zeta^{\frac{1}{2}} q_x^2 + \zeta^{-\frac{1}{2}} q_y^2}, \tag{69}$$

respectively. Here, n is the total density of the xz and yz bands only since we are not considering the xy band. The density-of-states mass is $m_{\rm DOS} = \sqrt{m_{\rm L} m_{\rm H}}$, the reduced mass is $\bar{m} = m_{\rm L} m_{\rm H}/(m_{\rm L} + m_{\rm H})$. Interestingly, the SP plasmon becomes isotropic in the long-wavelength limit.

In the PPA, the imaginary part of the density response function is expanded about the plasmon pole of the system [29]. Using the long-wavelength form of the density response function we obtain

$$\text{Im}\,\chi_i^{\rm PPA}(q,\omega) = -\frac{\pi\,\Omega_i}{2 v_q}\delta(\omega - \Omega_i(q)). \tag{70}$$

The fluctuation-dissipation theorem [29] allows us to then find the instantaneous structure factor

$$S_i^{\rm PPA}(\boldsymbol{q}) = -\frac{\hbar}{\pi n}\int_0^\infty \text{Im}\,\chi_i^{\rm PPA}(\boldsymbol{q},\omega) d\omega, \tag{71}$$

and then the interaction energy per electron in the ith broken symmetry state is given by

$$\frac{E_{\rm C}^i}{N} = \frac{1}{8\pi^2}\int d^2\boldsymbol{q}\; v_q\big[S_i^{\rm PPA}(\boldsymbol{q}) - 1\big]. \tag{72}$$

Although the long-wavelength PPA static structure factor gives a formally divergent interaction energy, the contribution to the interaction energy at each wave vector $|\boldsymbol{q}|$ has meaning in the long-wavelength limit $|\boldsymbol{q}| \ll k_{\rm F}$ [50]. We define the correlation energy per electron from transitions at wave vector $|\boldsymbol{q}|$, $E_{\rm C}^i(q)$, by the relationship

$$\frac{E_{\rm C}^i}{N} = \int_0^\infty \frac{E_{\rm C}^i(q)}{N} dq. \tag{73}$$

We find that the contribution to the interaction energy per electron at each wave vector $|\boldsymbol{q}|$ is

$$\frac{E_{\rm C}^{\rm OP}(q)}{N} = \frac{\hbar q^2}{4\pi^2 n}\sqrt{\frac{v_q n}{m_{\rm DOS}}}\left[\zeta^{1/4}\Xi\left(\frac{\zeta-1}{\zeta}\right)\right] - \frac{q v_q}{4\pi} \tag{74}$$

in the orbital-ordered state, and in the spin-ordered state is given by

$$\frac{E_{\rm C}^{\rm SP}(q)}{N} = \frac{\hbar q^2}{8\pi n}\sqrt{\frac{v_q n}{2\bar{m}}} - \frac{q v_q}{4\pi}, \tag{75}$$

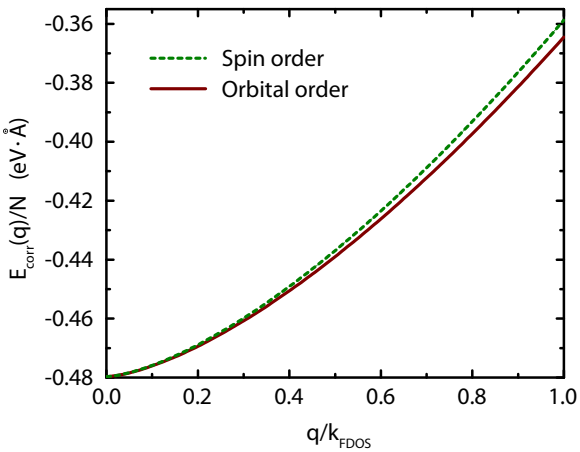

FIG. 3. The contribution to the correlation energy per electron from transitions with wave vector q is plotted for the orbital-ordered (solid brown) and spin-ordered (dashed green) broken symmetry states. [Compare to Eqs. (74) and (75), respectively.] The correlation energy is calculated within the plasmon-pole approximation and in a simplified model in which the circular xy band is absent. We have taken the total density to be 5×10^{12} cm^{-2}.

where $\Xi(x)$ is the complete elliptic integral of the second kind. The last term on the right hand side in both Eqs. (74) and (75) is proportional to the classical self-interaction energy of the plasmon density fluctuation at wavelength $2\pi/q$. The first term on the right hand side is the zero-point energy of each plasmon mode [50].

In Fig. 3 we plot Eqs. (75) and (74) against $|\boldsymbol{q}|$ in units of an effective density-of-states Fermi wave vector defined by $k_{\mathrm{FDOS}} = \sqrt{4\pi n/g}$, where $g = 2$ is the number of occupied spin-resolved bands in either the spin- or orbital-ordered states. The orbitally polarized phase is of lower energy as a result of the smaller zero-point plasmon energy at wave vector $|\boldsymbol{q}|$.

V. SUMMARY AND DISCUSSION

Orbital order is an interesting possibility in t_{2g} electron systems, even in the itinerant limit of doped d^0 materials with a small value for the number of electrons per metal site. We refer to the low-density t_{2g} systems as t_{2g} electron gases. The orbitally ordered t_{2g} electron gas is an electron nematic [51], a translationally invariant metallic phase with a spontaneously generated spatial anisotropy. In this paper we have developed and applied a theory of two-dimensional t_{2g} electron gases confined at a surface or interface by an external electric field, which accounts for transverse correlations induced by Coulombic electron-electron interactions using a random phase approximation, and optimizes the subband wave functions of the three t_{2g} two-dimensional bands by minimizing the total energy. In the present calculation we have assumed that the t_{2g} 2DEG has only one subband per flavor, but the formalism allows this approximation to be relaxed.

It is interesting to consider advantages and disadvantages of the approach described in this paper with other approaches that are also valuable in addressing the physics of t_{2g} electron gases. A density-functional theory (DFT) approach, for example, has the advantage of being able to account flexibly for structural rearrangements near interfaces which might play a role in some cases. On the other hand DFT has the disadvantage that it is technically difficult to accurately treat cases with a small number of electrons per unit cell where the most important physics occurs in a small part of a supercell Brillouin zone. In addition, DFT normally uses a generic approximate functional to describe exchange and correlation. In the case of t_{2g} systems it is clear that these approximations do not capture specific features in the exchange-correlation physics that are special to t_{2g} electron gases, for example the difference between the exchange and correlation energies of electrons in elliptical vs circular bands that we have discussed. We view the work described in this paper as complementary to efforts to unlock t_{2g} electron gas physics using DFT.

For definiteness, in our calculations we consider the case when the t_{2g} electrons are confined to an interface and also confined in a quantum well with a finite number of metal layers, N_l. Below a critical density that decreases with increasing N_l, only xy bands are occupied because they have smaller confinement energies. We find that orbital order occurs when the yz,xz elliptical band density is below a critical value and that it occurs over a broader range of total density for wider quantum wells. At very low elliptical band density spin order occurs in additional to orbital order.

Anisotropic magnetoresistance measurements of $LaAlO_3/SrTiO_3$ heterojunctions [52–54] indicate uniaxial anisotropy which spontaneously appears above a critical density at which the xz and yz bands start to be occupied and disappears when the xz and yz bands' density becomes large. The magnetic properties of these systems is not perfectly understood to date, but some theoretical analysis based on Hubbard-like model interactions [55–57] and Kondo models [58] has recently appeared. We point out that both the orbitally ordered as well as the orbitally and spin ordered phases we have found would introduce a uniaxial anisotropy in the system, and may explain these measurements.

Several other systems have shown indications of the Bloch-like [15] instability which drives the transition to orbital and spin order in the t_{2g} electron gas. Experimentally, some evidence for a ferromagnetic instability has been observed in transport studies of very clean low-density Si 2DEGs [17,18]. Spin ordering in these itinerant electron 2DEGs is supported by a large enhancement in the spin susceptibility as the density is lowered [59]. Meanwhile, in the multivalley semiconductor AlAs, where the valley degree-of-freedom is closely analogous to our t_{2g} 2DEG's band/orbital degree-of-freedom, large Coulomb-interaction enhancements of the valley susceptibility have been measured [60]. In addition, exchange-correlation energies are understood to play an important quantitative role in valley occupancy symmetry breaking in Si inversion layers [61,62]. Lastly, numerical studies of single-band 2DEG systems which include both disorder and the Coulomb interaction have found a magnetic ordered ground state [21,63]. Despite these studies, Bloch-like broken symmetry states have not been unambiguously observed to date. Our calculations suggest that Bloch-like instability to an orbital-ordered state may be present in thin-film $SrTiO_3$ heterojunctions.

The variational approach described in this paper can be applied to wide semiconductor quantum wells in which there is also a subtle interplay between correlations and subband wave functions and to Van der Waals heterostructures [64]. Although multiple orbitals are not often present near the Fermi energy, these layered materials have a weak electronic hopping amplitude in the confinement direction, and as a result many subbands are occupied even in relatively thin multilayers. Additionally, many van der Waals materials have been observed to be strongly interacting, often exhibiting diverse phenomena like charge-density wave instabilities [65], superconductivity [66], and negative compressibility [67].

ACKNOWLEDGMENTS

J.R.T. thanks Jeremy Levy, Lu Li, José Lorenzana, and Fengcheng Wu for interesting discussions. Work in Austin was supported by the DOE Division of Materials Sciences and Engineering under Grant No. DE-FG02-ER45118 and by the Welch foundation under Grant No. TBF1473. M.P. was supported by Fondazione Istituto Italiano di Tecnologia and the European Union's Horizon 2020 research and innovation programme under Grant Agreement No. 696656 "GrapheneCore1."

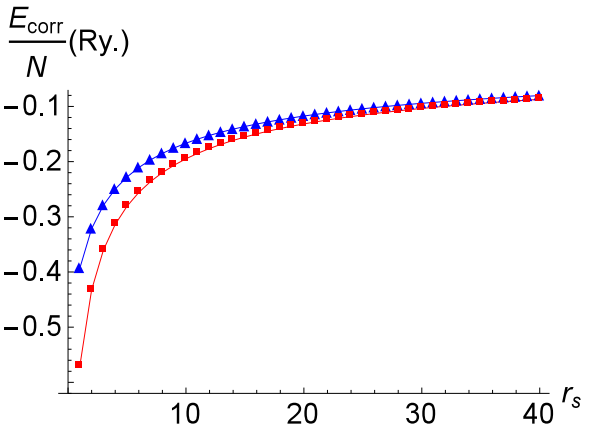

FIG. 4. A plot of the RPA correlation energy per electron (in units of effective Rydbergs) as the parameter r_s is varied from one to forty. Equation (A1) defines r_s in terms of the total electron density. The blue curve is for a single band isotropic 2DEG with equal populations of both spin species. The red curve is for a 2DEG with two identical isotropic bands with equal spin populations in both bands. Note that the bands are of different orbital content, and therefore interband scattering is negligible. The correlation energy per electron increases in magnitude with the number of occupied bands.

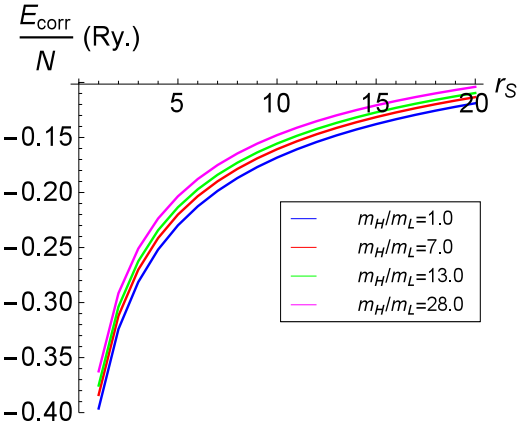

FIG. 5. A plot of the RPA correlation energy per electron (in units of effective Rydberg) for single band 2DEGs of varying band anisotropy defined by the ratio of the mass in the x direction, $m_{\rm H}$, and the mass in the y direction, $m_{\rm L}$. The correlation energy per electron is reduced in magnitude for increasing band anisotropy.

APPENDIX: THE RPA CORRELATION ENERGY DEPENDENCE ON NUMBER OF BANDS AND BAND ANISOTROPY

In this Appendix we explore the dependence of the RPA correlation energy on the number of bands with distinct orbital character and on the degree of band anisotropy. In Fig. 4 we examine how the correlation energy changes by the addition of a second identical isotropic band of effective mass $m^{\rm eff}$. We plot the correlation energy in units of effective Rydberg Ry. $= m^{\rm eff}$ry.$/\kappa^2$ where ry. $= 13.6$ meV is the bare Rydberg. The parameter r_s in this figure is defined in terms of the total 2DEG density n, which is distributed equally amongst either one or two bands,

$$r_s = \frac{m^{\rm eff}}{a_{\rm B}\kappa\sqrt{\pi n}}. \tag{A1}$$

Since the dielectric constant κ and the effective mass $m^{\rm eff}$ enter into the definition of both Ry. and r_s, the curves in Fig. 4 are independent of the exact numerical value of both κ and $m^{\rm eff}$. We find that the RPA correlation energy per electron is larger for the system with two bands.

In Fig. 5 we examine how the correlation energy of a single 2D band changes as the degree of anisotropy varies. We take the band to have an elliptical Fermi surface and a heavy mass $m_{\rm H}$ in the x direction and a light mass $m_{\rm L}$ in the y direction (exactly like the yz band of our model for $SrTiO_3$ in the main text). We plot the correlation energy in units of effective Rydberg Ry. $= \sqrt{m_{\rm H}m_{\rm L}}$ry.$/\kappa^2$. The parameter r_s in this figure is defined in terms of the total 2DEG density n,

$$r_s = \frac{\sqrt{m_{\rm H}m_{\rm L}}}{a_{\rm B}\kappa\sqrt{\pi n}}. \tag{A2}$$

We find that the correlation energy per electron is reduced as the degree of band anisotropy increases.

[1] J. B. Goodenough, Phys. Rev. **100**, 564 (1955).
[2] E. O. Wollan and W. C. Koehler, Phys. Rev. **100**, 545 (1955).
[3] J.-G. Cheng, Y. Sui, J.-S. Zhou, J. B. Goodenough, and W. Su, Phys. Rev. Lett. **101**, 087205 (2008).
[4] J.-Q. Yan, J.-S. Zhou, and J. B. Goodenough, Phys. Rev. Lett. **93**, 235901 (2004).
[5] J.-S. Zhou, J. B. Goodenough, J.-Q. Yan, J.-G. Cheng, K. Matsubayashi, Y. Uwatoko, and Y. Ren, Phys. Rev. B **80**, 224422 (2009).
[6] J. Mannhart and D. G. Schlom, Science **327**, 1607 (2010).
[7] A. P. Kajdos, D. G. Ouellette, T. A. Cain, and S. Stemmer, Appl. Phys. Lett. **103**, 082120 (2013).
[8] Y. Kozuka, M. Kim, H. Ohta, Y. Hikita, C. Bell, and H. Y. Hwang, Appl. Phys. Lett. **97**, 222115 (2010).
[9] S. Stemmer and S. J. Allen, Annu. Rev. Mater. Res. **44**, 151 (2014).
[10] J. A. Sulpizio, S. Ilani, P. Irvin, and J. Levy, Annu. Rev. Mater. Res. **44**, 117 (2014).
[11] T. Mizokawa and A. Fujimori, Phys. Rev. B **54**, 5368 (1996).
[12] M. Mochizuki and M. Imada, J. Phys. Soc. Jpn. **73**, 1833 (2004).
[13] In the low-density limit the leading order contribution to the interaction energy per electron of a single-band electron gas with Coulomb interactions goes like $1/r_S \propto n^{1/2}$ (see for example Ref. [29]). Meanwhile the interaction energy per electron obtained using Hubbard interactions is $\propto n$, which can be seen by applying first-order perturbation theory. Further quantitative understanding can be found by considering the closely related model of a dilute Fermi gas with strong short-range interactions. In the low-density limit the leading contribution to the interaction energy has been found to be $\propto n$ up to a logarithmic correction [J. R. Engelbrecht, M. Randeria, and L. Zhang, Phys. Rev. B **45**, 10135(R) (1992)].

[14] J. R. Tolsma, A. Principi, R. Asgari, M. Polini, and A. H. MacDonald, Phys. Rev. B **93**, 045120 (2016).

[15] F. Bloch, Z. Physik **57**, 545 (1929).

[16] D. P. Young, D. Hall, M. E. Torelli, Z. Fisk, J. L. Sarrao, J. D. Thompson, H.-R. Ott, S. B. Oseroff, R. G. Goodrich, and R. Zysler, Nature (London) **397**, 412 (1999).

[17] S. A. Vitakalov, H. Zheng, K. M. Mertes, M. P. Sarachik, and T. M. Klapwijk, Phys. Rev. Lett. **87**, 086401 (2001).

[18] A. A. Shashkin, S. V. Kravchenko, V. T. Dolgopolov, and T. M. Klapwijk, Phys. Rev. Lett. **87**, 086801 (2001).

[19] N. Teneh, A. Yu. Kuntsevich, V. M. Pudalov, and M. Reznikov, Phys. Rev. Lett. **109**, 226403 (2012).

[20] K. Takashina, Y. Niida, V. T. Renard, B. A. Piot, D. S. D. Tregurtha, A. Fujiwara, and Y. Hirayama, Phys. Rev. B **88**, 201301(R) (2013).

[21] V. T. Renard, B. A. Piot, X. Waintal, G. Fleury, D. Cooper, Y. Niida, D. Tregurtha, A. Fujiwara, Y. Hirayama, and K. Takashina, Nat. Commun. **6**, 7230 (2015).

[22] Y. Zhang and S. Das Sarma, Phys. Rev. B **72**, 115317 (2005).

[23] C. Attaccalite, S. Moroni, P. Gori-Giorgi, and G. B. Bachelet, Phys. Rev. Lett. **88**, 256601 (2002).

[24] B. Tanatar and D. Ceperley, Phys. Rev. B **39**, 5005 (1989).

[25] P. Hohenberg and W. Kohn, Phys. Rev. **136**, B864 (1964).

[26] W. Kohn and L. J. Sham, Phys. Rev. **140**, A1133 (1965).

[27] D. C. Langreth and J. P. Perdew, Phys. Rev. B **21**, 5469 (1980).

[28] J. P. Perdew, K. Burke, and M. Ernzerhof, Phys. Rev. Lett. **77**, 3865 (1996).

[29] G. F. Giuliani and G. Vignale, *Quantum Theory of the Electron Liquid* (Cambridge University Press, Cambridge, 2005).

[30] R. O. Jones and O. Gunnarsson, Rev. Mod. Phys. **61**, 689 (1989).

[31] J. Heyd, G. E. Scuseria, and M. Ernzerhof, J. Chem. Phys. **118**, 8207 (2003).

[32] J. Perdew, M. Ernzerhof, and K. Burke, J. Chem. Phys. **105**, 9982 (1996).

[33] Z. S. Popovic, S. Satpathy, and R. M. Martin, Phys. Rev. Lett. **101**, 256801 (2008).

[34] G. Khalsa and A. H. MacDonald, Phys. Rev. B **86**, 125121 (2012).

[35] S. E. Park and A. J. Millis, Phys. Rev. B **87**, 205145 (2013).

[36] K. Ueno, S. Nakamura, H. Shimotani, A. Ohtomo, N. Kimura, T. Nojima, H. Aoki, Y. Iwasa, and M. Kawasaki, Nat. Mater. **7**, 855 (2008).

[37] A. Joshua, S. Pecker, J. Ruhman, E. Altman, and S. Ilani, Nat. Commun. **3**, 1129 (2012).

[38] Santosh Raghavan, S. James Allen, and Susanne Stemmer, Appl. Phys. Lett. **103**, 212103 (2013).

[39] I. Aliaj, I. Torre, V. Miseikis, E. di Gennaro, A. Sambri, A. Gamucci, C. Coletti, F. Beltram, F. M. Granozio, M. Polini, V. Pellegrini, and S. Roddaro, APL Materials **4**, 066101 (2016).

[40] Y. Lee, C. Clement, J. Hellerstedt, J. Kinney, L. Kinnischtzke, X. Leng, S. D. Snyder, and A. M. Goldman, Phys. Rev. Lett. **106**, 136809 (2011).

[41] P. Moetakef, C. A. Jackson, J. Hwang, L. Balents, S. J. Allen, and S. Stemmer, Phys. Rev. B **86**, 201102(R) (2012).

[42] R. Chen, S. Lee, and L. Balents, Phys. Rev. B **87**, 161119(R) (2013).

[43] S. J. Allen, B. Jalan, S. Lee, D. G. Ouellette, G. Khalsa, J. Jaroszynski, S. Stemmer, and A. H. MacDonald, Phys. Rev. B **88**, 045114 (2013).

[44] A. Faridi, R. Asgari, and A. Langari, Phys. Rev. B **93**, 235306 (2016).

[45] Although the long-wavelength low-temperature static dielectric constant of bulk $SrTiO_3$ is in the tens of thousands [A. S. Barker Jr. and M. Tinkham, Phys. Rev. **125**, 1527 (1962)] because of the presence of a soft LO phonon mode near the Γ point, the effective dielectric constant which screens electron-electron interactions is expected to be substantially smaller. The electronic transitions which contribute to the ground-state energy in the t_{2g} model are on the scale of a few hundred meV, much larger than the soft-phonon mode energy which is closer to a few meV [Y. Yamada and G. Shirane, J. Phys. Soc. Jpn. **26**, 396 (1969)]. Screening by this mode is therefore weak. Furthermore, the LO phonon mode is soft only in close vicinity to the Γ point. Even static electric fields are ineffectively screened by this mode unless they are constant over distances which greatly exceed a lattice constant. Based on these considerations, we think that the effective dielectric constant to be included in electron-electron interaction calculations is closer to $\kappa \sim 15$, similar to small-gap covalent semiconductors. At liquid helium temperatures the dielectric constant of bulk $SrTiO_3$ is $\kappa \sim 10$ in the range 2–40 meV and $\kappa \sim 7$ above 40 meV [R. C. Neville, B. Hoeneisen and C. A. Mead, J. Appl. Phys. **43**, 2124 (1972)]. For completeness we note that a recent *ab initio* calculation within the local density approximation (LDA) predicted that the static long-wavelength dielectric constant of $SrTiO_3/LaAlO_3$ was strongly suppressed as the 2DEG density increased, $\kappa \sim 50$ for $n \sim 10^{14}$.

[46] E. Anderson, Z. Bai, C. Bischof, S. Blackford, J. Demmel, J. Dongarra, J. Du Croz, A. Greenbaum, S. Hammarling, A. McKenney, and D. Sorensen, *LAPACK Users' Guide* (Society for Industrial and Applied Mathematics, Philadelphia, 1999).

[47] W. Press, S. A. Teukolsky, W. T. Vetterling, and B. P. Flannery, *Numerical Recipes in C* (Cambridge University Press, Cambridge, 2002).

[48] The RPA can be viewed as the leading term in an expansion in N_f^{-1}, where N_f is the number of Fermion bands, and we can expect that it becomes more accurate when the number of Fermion species increases. This observation suggests that the RPA is a reasonable starting point for treating Coulomb correlations in the six band t_{2g} 2DEG model.

[49] F. Pederiva, E. Lipparini, and K. Takayanagi, Europhys. Lett. **40**, 607 (1997).

[50] D. Pines and P. Noziéres, *The Theory of Quantum Liquids* (W. A. Benjamin, Inc., New York, 1966).

[51] E. Fradkin, S. A. Kivelson, M. J. Lawler, J. P. Eisenstein, and A. P. Mackenzie, Annu. Rev. Condens. Matter Phys. **1**, 153 (2010).

[52] M. Ben Shalom, C. W. Tai, Y. Lereah, M. Sachs, E. Levy, D. Rakhmilevitch, A. Palevski, and Y. Dagan, Phys. Rev. B **80**, 140403(R) (2009).

[53] A. Annadi, Z. Huang, K. Gopinadhan, X. Renshaw Wang, A. Srivastava, Z. Q. Liu, H. Harsan Ma, T. P. Sarkar, T. Ventatesan, and Ariando, Phys. Rev. B **87**, 201102(R) (2012).

[54] A. Joshua, J. Ruhman, S. Pecker, E. Altman, and S. Ilani, Proc. Nat. Acad. Sci. **110**, 9633 (2013).

[55] S. Banerjee, Onur Erten, and M. Randeria, Nat. Phys. **9**, 626 (2013).

[56] M. H. Fischer, S. Raghu, and E.-A. Kim, New J. Phys. **15**, 023022 (2013).

[57] G. Chen and L. Balents, Phys. Rev. Lett. **110**, 206401 (2013).
[58] J. Ruhman, A. Joshua, S. Ilani, and E. Altman, Phys. Rev. B **90**, 125123 (2014).
[59] V. M. Pudalov, M. E. Gershenson, H. Kojima, N. Butch, E. M. Dizhur, G. Brunthaler, A. Prinz, and G. Bauer, Phys. Rev. Lett. **88**, 196404 (2002).
[60] O. Gunawan, Y. P. Shkolnikov, K. Vakili, T. Gokmen, E. P. De Pootere, and M. S. Shayegan, Phys. Rev. Lett. **97**, 186404 (2006).
[61] W. L. Bloss, S. C. Ying, and J. J. Quinn, Phys. Rev. B **23**, 1839 (1981).
[62] W. L. Bloss, L. J. Sham, and V. Vinter, Phys. Rev. Lett. **43**, 1529 (1979).
[63] G. Benenti, G. Caldara, and D. L. Shepelyansky, Phys. Rev. Lett. **86**, 5333 (2001).
[64] A. K. Geim and I. V. Grigorieva, Nature (London) **499**, 419 (2013).
[65] X. Xi, L. Zhao, Z. Wang, H. Berger, L. Forró, J. Shan, and K. F. Mak, Nat. Nanotechnol. **10**, 765 (2015).
[66] J. M. Lu, O. Zheliuk, I. Leemakers, N. F. Q. Yuan, U. Zeitler, K. T. Law, and J. T. Ye, Science **350**, 1353 (2015).
[67] S. Larentis, J. R. Tolsma, B. Fallahazad, D. C. Dillen, K. Kim, A. H. MacDonald, and E. Tutuc, Nano. Lett. **14**, 2039 (2014).